# MASTERARBEIT

## Towards Long Distance

## Quantum State Teleportation

Verfasser:

## William Naylor BSc (Hons)

Angestrebter akademischer Grad:

## Master of Sience (MSc)

Wien, 2010.

| | |
|---|---|
| Studienkennzahl lt. Studienblatt: | A 066 876 |
| Matrikelnummer: | 0867825 |
| Studienrichtung lt. Studienblatt: | Masterstudium Physik UG2002 |
| Betreuerin / Betreuer: | o. Univ. Prof. Dr. Anton Zeilinger |

# Contents

# 0. Zusammenfassung/Abstract

## 0.1. Zusammenfassung

In dieser Masterarbeit wurde die Vorbereitung zu einem Quantenteleportations-Experiment über lange Distanz präpariert, welches Anfang nächsten Jahres, zwischen den Kanarischen Inseln La Palma und Teneriffa durchgeführt werden wird. Die Verbindung zwischen den zwei Inseln ist ein optischer ,,free-space''- Link mit insgesamt 144 km Länge. Quantenteleportation wurde schon von vielen anderen Arbeitsgruppen durchgeführt, erstmals 1997 [8]. Vor kurzem ist ein Teleprepparationsexperiment (siehe Kapitel 3) über 16 km ,,free-space'' gelungen [22]. Des Weiteren wurde im Jahr 2007 mit Mitarbeitern der gleichen Gruppe, mit dem gleichen Kommunikationskanal, ein Quanten-Schlüsseltausch über 144km durchgeführt [46].

Diese Arbeit besteht aus der Konstruktion und Charakterisierung eines Setups in Wien, welches auf den Kanarischen Inseln zum Einsatz kommen wird. Wir teleportieren ein Qubit, realisiert durch die Polarisationszustände eines Photons. Zum Erzielen der Verschränkung wird spontane parametrische Down-Conversion verwendet. Die Optimierung dieses Prozesses ist von zentraler Bedeutung für das Experiment. Zusätzlich ist der Aufbau so geplant, dass das Photon sowohl im Fock-Zustand als auch im kohärenten Zustand teleportiert werden kann, wobei besonders die Verwendung des kohärenten Zustandes sehr hohe Zählraten erlaubt. Auf diese Weise können wir die Zählraten anpassen, um am Effektivsten eine Teleportation im Quantenzustand zu demonstrieren.

Diese Arbeit wurde zwischen Februar 2009 und Mai 2010 fertiggestellt.

## 0.2. Abstract

In this masters thesis we present a body of work towards a long distance quantum teleportation experiment to be completed in the near future between two of the Canary Islands: La Palma and Tenerife. The link between the islands is an optical free-space link with a total distance of 144 km. Previously a number of teleportation experiments have been realised, the first in 1997 [8]. Recently Jin et. al. performed a free-space teleprepreparation (see Ch. 3) experiment over 16 km [22]. In addition quantum key distribution over 144 km was completed (over the same link that is proposed for this work and by members of the same group) in 2007 [46].

This work consists of the construction and characterisation of a setup in Vienna, Austria that is to be used in the Canary Islands. We teleport a qubit realised as the polarisation state of a photon. We use spontaneous parametric down-conversion to create entanglement and thus the optimisation of this process is of central importance to this work. In addition the setup is designed such that the photon to be teleported may be in either a Fock state or a coherent state. In particular using the coherent state allows for very high count rates and thus we investigate how we can adjust these rates so as to most effectively demonstrate quantum state teleportation. The present work was completed between February 2009 and May 2010.

# 1. Motivation

In classical physics a system can be fully characterised by measuring its properties. Furthermore one can investigate the parts of the system in ever increasing detail and still fully characterise the total system simply by measuring the properties of all the subsystems. That is, information about the whole system is the sum of the information about the parts. This is not the case in quantum mechanics. The results of measurements on a system do not, in general, characterise the system as completely as in classical mechanics and it may not be possible to break up a system into subsystems without losing information about the complete system. Thus, in contrast to classical physics, information about the whole system is not the sum of the information about its constituent parts.

A polynomial increase in the number of subsystems (that is input resources) within a quantum system can result in an exponential increase in the total system size, measured in units of possible states. These 'additional' states available to many-body quantum systems are entangled states. These states can be utilised in a number of tasks, dramatically increasing their efficiency.

The points given above form the broad motivation for almost all experiments within the field of quantum information science. I shall now elaborate on these and show their connection to this work.

The first point illustrates the departure of the theory of quantum mechanics from any previous classical theory. However the features of classical mechanics, in particular reality and locality, seem so obviously and intuitively true that many people believe they are integral to the world around us, even though they are not all present within quantum mechanics. In 1964 Bell presented a paper which mathematically showed that local realistic theories give different results to quantum mechanics [4]. Then Clauser, Horne, Shimony and Holt proposed a method of experimentally testing the counter-intuitive predictions of quantum mechanics against the aforementioned classical principles [12]. Since then a number of experiments have confirmed the predictions of quantum mechanics. In addition many other experiments have highlighted particularly counter intuitive situations, inspired by and consistent with quantum theory, that arise in nature. An obvious extension to these current experiments is extending the range over which such experiments are carried out. This could be achieved, on an impressive scale, by conducting experiments in space using satellites. The high quality quantum state operations combined with the challenging link conditions planned for this experiment represent a step towards any such satellite based experiments [24].

Despite it being easily possible to envisage a classical teleportation protocol, the nature, particularly within popular culture, of teleportation makes this experiment an exciting proposal. A telescope, sitting high above the clouds on Tenerife, one of the Canary Islands, usually used for looking up to the stars will instead be pointed to the horizon to collect light emitted from a telescope on a separate island, La Palma, 144 km away. In doing so the quantum state of a photon will be teleported between the two islands. Given the pop culture connotations, the location and equipment used and the scales involved it is hoped this work can capture the imaginations of at least a section of the general public, as well as those of scientists, thus going a long way to illustrate the strange workings of our world

The second point states that, in certain situations, exploiting the quantum mechanical behaviour of systems can result in a dramatic reduction in the difficulty in performing such tasks. The direct application of this idea leads to the field of quantum computation [29]. Possibly the most famous example of a quantum mechanically enhanced algorithm is Shor's Algorithm [16], where the prime factors of an integer can be found in polynomial time, exponentially faster than any known classical algorithm. This particular task is very important as its difficulty in classical mechanics forms the basis for the majority of internet encryption schemes. In addition the application of quantum principles to cryptography allows cryptographic information to be secure in principle rather than simply difficult to decode, as in classical schemes. In both cases it would be advantageous to be able to distribute quantum systems over large distances and ultimately over a global quantum network. A realistic means of creating such a network would utilise free-space links between ground stations and satellites, similar to the ideas given above for fundamental tests in space. In this work a four photon experiment is prepared that is both bright enough and has sufficiently low error rate to be able to successfully demonstrate quantum teleportation over a 144 kilometre free-space link with better fidelity than any possible classical scheme thus this also represents a step forward in the quest to create such a satellite based global quantum network where such bright sources with low error rate would also be essential.

# 2. Ingredients of quantum teleportation

In this chapter we introduce some of the basic tools and definitions that are utilised in the work that follows. First quantum states and their representation are given, then entanglement is introduced and finally the no cloning theorem is stated.

## 2.1. Quantum states

A quantum state is a vector in Hilbert space, this vector is used to represent the feature of the physical world that is under consideration, thus we also term the features of the world under consideration quantum states. Of special interest are systems with only two orthogonal states as they are the simplest systems with non-trivial evolution and provide the quantum analogue to the classical bit (a system with two possible states, noted **0** and **1**). In the Dirac notation of quantum mechanics these two states are represented by the vectors $|0\rangle$ and $|1\rangle$; it is important to note that $|0\rangle$ and $|1\rangle$ are orthogonal states, that is neither state contains a component of the other. While the classical bit has only two possible states, **0** or **1**, the quantum bit may exist in infinitely many different states, given by

$$|\psi\rangle = \alpha |0\rangle + \beta |1\rangle , \tag{2.1}$$

where $\alpha$ and $\beta$ are complex numbers with the constraint[1] $|\alpha|^2 + |\beta|^2 = 1$. Equation 2.1 represents the maximum possible information we may have about a qubit, however, if this qubit has interacted with another system, it may not even be possible to give such a description (i.e. this much information may not be available). In such cases the state may not be written as a simple sum of kets as in Eq. 2.1, we instead use the density operator. Thus any qubit may be written in the form;

$$\rho = \frac{1}{2}\big(\mathbf{1} + \mathbf{r} \cdot \vec{\sigma}\big) , \tag{2.2}$$

---

[1] $|\alpha|^2$ and $|\beta|^2$ are the probabilities that that particle will be found in states $|0\rangle$ and $|1\rangle$ respectively. Because the particle must be in one of these states when measured in this basis the sum of these probabilities must be unity.

where $\mathbf{r}$ is a real vector in three-space with $|\mathbf{r}| \leq 1$ and the $\sigma_i$ are the Pauli matrices given by,

$$\sigma_1 = \begin{pmatrix} 0 & 1 \\ 1 & 0 \end{pmatrix}, \sigma_2 = \begin{pmatrix} 0 & -i \\ i & 0 \end{pmatrix} \text{ and } \sigma_3 = \begin{pmatrix} 1 & 0 \\ 0 & -1 \end{pmatrix}. \tag{2.3}$$

The qubit states given above can be described visually as points on, or within, the Bloch sphere (known as the Poincaré sphere when describing classical polarisation states) shown in Figure 2.1. In this work qubits are realised physically using the polarisation states of photons, thus we generally use the nomenclature of polarisation states. Figure 2.1a. shows the three mutually unbiased polarisation bases: H/V, D/A and R/L. These are the bases which are composed of the orthogonal states $|H\rangle$ and $|V\rangle$, representing horizontal and vertical polarisation; $|D\rangle$ and $|A\rangle$, diagonal and anti-diagonal; and $|R\rangle$ and $|L\rangle$, right-hand and left-hand circular polarisation. In Eq. 2.2 the components $(r_1, r_2$ and $r_3)$ of vector $\mathbf{r}$ are the projections of $\mathbf{r}$ along the $|H\rangle$, $|D\rangle$ and $|R\rangle$ axes respectively.
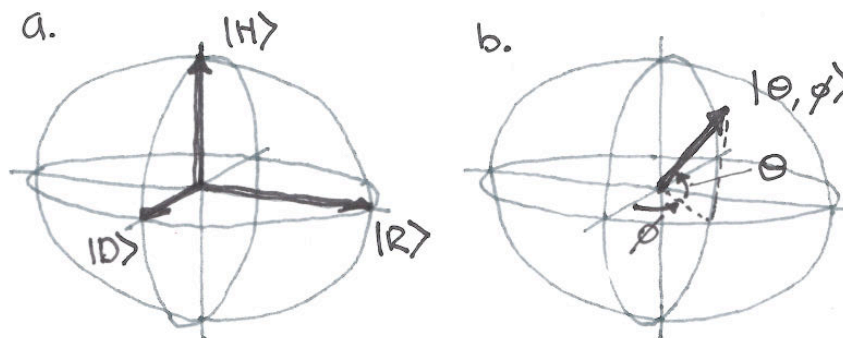


**Figure 2.1.:** The Bloch sphere. Figure 2.1a shows three mutually unbiased basis vectors, $|H\rangle$, $|D\rangle$ and $|R\rangle$. 2.1b shows an arbitrary pure quantum state of the form of Eq. 2.4.

From Eq. 2.2 we can picture two extreme cases. First where $|\mathbf{r}| = 0$ we obtain states that are completely incoherent mixtures of the two orthogonal states (and this is true in any basis). Such states lie exactly in the centre of the Bloch sphere and can arise when the system is entangled with another system, see Chap. 2.1.1. In the opposite case, $|\mathbf{r}| = 1$, the phase between the two orthogonal basis states is exactly defined, as in Eq. 2.1. These states are pure states and represent a state that has no entanglement to any other system. In the case of pure states Eq. 2.1 can be redefined as

$$|\psi\rangle = \cos(\theta/2)|0\rangle + \sin(\theta/2)e^{i\phi}|1\rangle , \tag{2.4}$$

where $\theta$ and $\phi$ are real quantities. The angles $\theta$ and $\phi$ given in Eq. 2.4 represent the polar and azimuthal angles on the Bloch sphere respectively as shown in Figure 2.1b.

## 2.1.1. Entanglement

Imagine a set of *independent* particles, 1, 2, ... in states $|a\rangle_1$, $|b\rangle_2$, ... . The state of the all particles, $|\text{One}\rangle_{12...}$, is simply the outer product of all the states

$$|\text{One}\rangle_{12...} = |a\rangle_1 \otimes |b\rangle_2 \otimes ... . \tag{2.5}$$

We may further imagine another possible state of the system where all the particles are in different states $|\alpha\rangle_1$, $|\beta\rangle_2$, ... .

$$|\text{Two}\rangle_{12...} = |\alpha\rangle_1 \otimes |\beta\rangle_2 \otimes ... . \tag{2.6}$$

Now the superposition principle of quantum mechanics states *'whenever the system is definitely in one state we can consider it as being party in each of two or more states. ... Conversely any two or more states may be superposed to give a new state.'* [13]. Thus a third possible state is

$$|\text{Three}\rangle_{12...} = \frac{1}{\sqrt{2}} \big( |\alpha\rangle_1 \otimes |\beta\rangle_2 \otimes ... + |a\rangle_1 \otimes |b\rangle_2 \otimes ... \big) . \tag{2.7}$$

In all cases the total state is simply a vector in a Hilbert space that is the outer product of the hilbert spaces of the constituent states, that is $\mathcal{H}_{12...} = \mathcal{H}_1 \otimes \mathcal{H}_2 \otimes ...$, where subscript indices follow the convention above. However this new state, $|\text{Three}\rangle_{12...}$, exhibits a number of different qualities to the first two.

As stated in the first two cases the particles are independent may be measured in arbitrary bases without effecting one another. However measurement of the state of particle 1 in the third case will pick out a single part of the sum in Eq. 2.7 thus changing the states of all the other particles. We thus see, in states of this type, the particles are correlated in some way. Such correlations are a hallmark of quantum entanglement.

In 1935 Erwin Schrödinger stated that entanglement was *'the characteristic trait of quantum mechanics'*, [42]. In the same year Albert Einstein, Boris Podolski and Nathan Rosen used entanglement in an attempt to show the incompleteness of quantum theory [15]. Twenty-nine years later John Bell [4] showed that it was possible to test the completeness of quantum theory. Clauser, Horne, Shimony and Holt using this idea gave a bound for the maximum possible value of a set of measurements that any local realistic theory[2] could give where with the same set of measurements quantum mechanics predicts a value in excess of the local realistic bound [12]. Since these works a number of experiments have shown that the local realistic bound is indeed exceeded [17, 48], although a definitive (i.e. 'loophole free') experiment has not yet been performed. The details of this

---

[2]There are actually three assumptions Bell used in deriving his inequality, these are (as given by Scheidl et. at. [41]): 'realism (objects possess definite properties prior to and independent of observation), locality (space-like separated events cannot causally influence each other), and freedom of choice (the choice of measurement settings is free or random).'

argument are not essential to this work however the correlations between entangled particles used to exceed the local realistic bound are of central importance. Thus we use this interesting situation as a means of illustrating the nature of two qubit entanglement.

Imagine a situation as in Fig. 2.2 where we have a twin source of particles and two experimenters, Alice and Bob[3]. Each experimenter has a measuring device that can measure in one of two different bases and has two possible measurement results, the value '+1' is given for one result and '-1' for the other result.
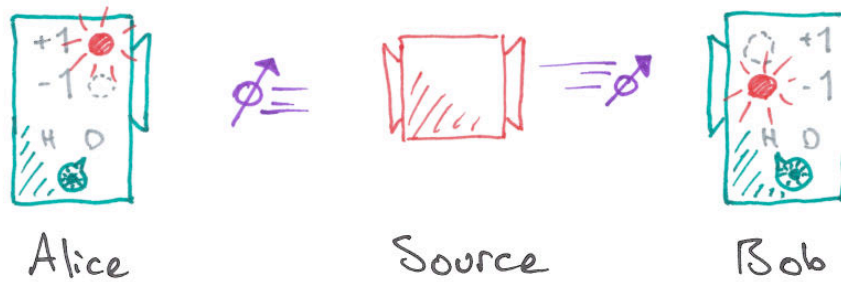


**Figure 2.2.:** Hypothetical setup for testing quantum correlations. A source produces two state particles that are sent to experimenters Alice and Bob who can independently choose between one of two bases in which to measure the qubits. They then record a value of +1 or -1 depending on the measurement result.

We may define a variable $S$ as

$$S = E(a,b) - E(a,b') + E(a',b) + E(a',b') \,, \qquad (2.8)$$

where $E(a,b)$ is the average correlation between a measurement at Alice with setting $a$ and a measurement at Bob with setting $b$. $a'$ and $b'$ correspond to measurements at Alice and Bob respectively in their other measurement bases of their measuring devices. The correlation $E(a,b)$ is the probability of recording the same result, $P_\parallel$, minus the probability of recording the opposite result, $P_\perp$,

$$E(a,b) = P_\parallel - P_\perp \,. \qquad (2.9)$$

For a local realistic theory we may maximise Eq. 2.8 by having the particles give measurement results of '+1' for all measurements, thus we have $S = 2$. The CHSH inequality [12] gives $-2 \leq S \leq 2$ as the bound for any local realistic theory. However if we were to use an entangled source the particles and for definiteness we will say they are in the singlet state[4], $(|H\rangle_1 |V\rangle_2 - |V\rangle_1 |H\rangle_2)/\sqrt{2}$ . And if Alice uses measurement settings of 0 deg. and 45 deg. and Bob uses 22.5 deg. and 67.5 deg. we have

---

[3]This work takes inspiration from a lecture given by David Mermin [35].

[4]Where, as in the following equation, an outer-product is obvious we will omit its symbol.

$$S = (-1)/\sqrt{2} - (+1)/\sqrt{2} + (-1)/\sqrt{2} + (-1)/\sqrt{2} \tag{2.10}$$

$$= -2\sqrt{2}\,, \tag{2.11}$$

where we have used $E(a,b) = -\cos(a-b)$, as given by quantum mechanics, illustrating that the correlations of maximally entangled particles are stronger than those possible with any local realist theory.

The singlet state given above is one of the four Bell states. These states are two-particle maximally entangled qubits that form a complete basis for any two particle qubit system. In the work to follow we use these states often and the following notation is used:

$$|\Psi_\pm\rangle \equiv \frac{1}{\sqrt{2}}\big(\,|\text{H}\rangle_1\,|\text{V}\rangle_2 \pm |\text{V}\rangle_1\,|\text{H}\rangle_2\,\big) \tag{2.12}$$

$$|\Phi_\pm\rangle \equiv \frac{1}{\sqrt{2}}\big(\,|\text{H}\rangle_1\,|\text{H}\rangle_2 \pm |\text{V}\rangle_1\,|\text{V}\rangle_2\,\big)\,. \tag{2.13}$$

## 2.1.2. No cloning theorem

Arguably the single most important theorem for teleportation is the no cloning theorem of Zurek and Wooters [50]. The theorem states that it is not possible to reproduce an unknown quantum state (unknown to the experimenter trying to reproduce the state).

Imagine we have a universal quantum cloning machine. This would take a state and produce two copies, thus for a horizontally polarised photon the effect of the machine may be written

$$|\text{H}\rangle \rightarrow |\text{H}\rangle\,|\text{H}\rangle\,. \tag{2.14}$$

Similarly for vertical polarisation we have

$$|\text{V}\rangle \rightarrow |\text{V}\rangle\,|\text{V}\rangle\,. \tag{2.15}$$

Now if we use our cloning machine to clone diagonal polarisation

$$|\text{D}\rangle = \frac{1}{\sqrt{2}}\big(|\text{H}\rangle + |\text{V}\rangle\big) \rightarrow \frac{1}{\sqrt{2}}\big(|\text{H}\rangle\,|\text{H}\rangle + |\text{V}\rangle\,|\text{V}\rangle\big) \tag{2.16}$$

however

$$|\text{D}\rangle\,|\text{D}\rangle = \frac{1}{2}\big(|\text{H}\rangle + |\text{V}\rangle\big) \otimes \big(|\text{H}\rangle + |\text{V}\rangle\big) \tag{2.17}$$

$$= \frac{1}{2}\big(|\text{H}\rangle\,|\text{H}\rangle + |\text{H}\rangle\,|\text{V}\rangle + |\text{V}\rangle\,|\text{H}\rangle + |\text{V}\rangle\,|\text{V}\rangle\big)\,, \tag{2.18}$$

which is clearly not the output of the cloning machine, thus no universal cloning machine may exist.

# 3. Quantum state teleportation

In this work we define teleportation as the exact reproduction of a quantum system at a distant point in space and time without simply moving the original system between the two points. These two points will be denoted A and B with two parties, Alice and Bob, working at the points denoted by their names. A third party, Victor, who will have agents at both locations, A and B, is utilised to verify that the teleportation was successfully completed. It is noted that Victor is not necessary in the actual teleportation, only to verify the result. Clearly the object to be teleported may carry information, and thus teleportation is bound by the speed of light i.e. instantaneous teleportation is not physically possible, moreover the time that it takes to complete the teleportation protocol will not be a factor in deciding if the teleportation was successful.

A simple scheme for teleportation world be for Alice to measure the system to be teleported at location A then send the results of those measurements to Bob at B who would then build a replica, thus 'teleporting' the system from A to B to the best possible accuracy of the measurement and reproduction. In this scheme it is not important what Alice does with her system after it is measured. However an exact and complete measurement (in the classical sense) of a system by Alice is not possible. Equally the scheme above would equate to the cloning of a quantum state which, as given in Chapter 2, is not possible.

In 1993 Bennett et. al. [5] proposed a scheme for the teleportation of a quantum state. Since then a number of variations on this scheme have been proposed and realised. In this chapter we introduce the teleportation protocol proposed by Bennett et. al. and summarise important previous experimental realisations.

## 3.1. Theoretical proposal for quantum teleportation

### 3.1.1. Qubit teleportation

First, as in the original paper, we shall discuss the two state teleportation protocol and then generalise to N-state quantum teleportation. To begin Alice receives the unknown quantum state, which, for verification reasons, is given to her by Victor, who will have noted the state in which it was prepared. Additionally she receives one qubit of a maximally entangled pair while Bob receives the other qubit of that maximally entangled pair. This is shown in Fig. 3.1.

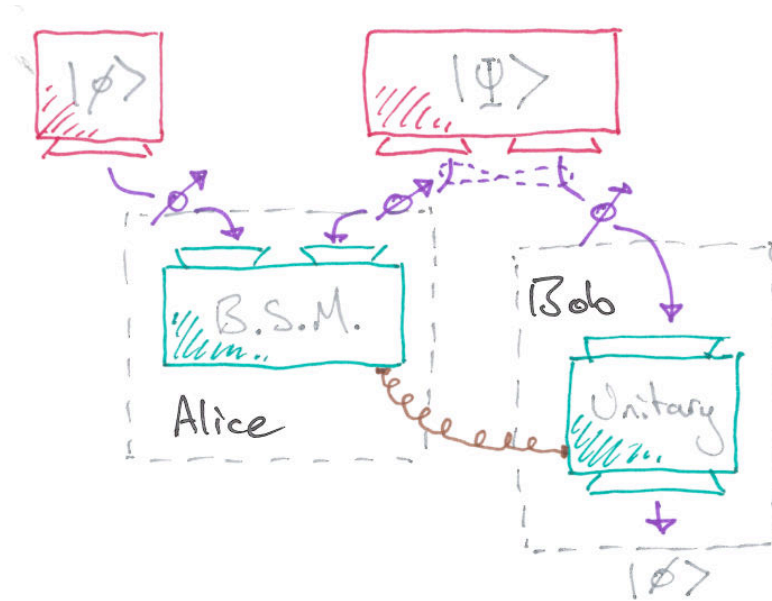The unknown quantum state to be teleported is denoted

**Figure 3.1.:** Schematic representation of the teleportation protocol. The input state and a singlet state are created then Alice performs a Bell state measurement on her two particles. Bob then performs a unitary operation on his particle conditional on the measurement result of Alice. The output state from Bob is then in the same state as the original input state and thus teleportation is achieved .

$$|\phi\rangle_1 = \alpha \, |\mathrm{H}\rangle_1 + \beta \, |\mathrm{V}\rangle_1 \ , \tag{3.1}$$

where the subscript denotes the particle number. We assume, as will be the case in the experiment, that the maximally entangled pair is in the singlet state. Thus the total state of all three particles is

$$|\Psi\rangle_{123} = \big(\alpha \, |\mathrm{H}\rangle_1 + \beta \, |\mathrm{V}\rangle_1\big) \otimes \frac{1}{\sqrt{2}} \big( |\mathrm{H}\rangle_2 \, |\mathrm{V}\rangle_3 - |\mathrm{V}\rangle_2 \, |\mathrm{H}\rangle_3 \big) \ . \tag{3.2}$$

Now Alice jointly measures the two particles that she has. She does this in a maximally entangled basis, thus the entanglement between particles 2 and 3 is shifted to entanglement between particles 1 and 2 (as after the measurement they must be in one of the eigenstates of the measurement: a maximally entangled state). For a pair of qubits a maximally entangled basis is the Bell basis, thus Alice performs a Bell state measurement on her two particles. Written in this basis the state $|\Psi\rangle_{123}$ takes the form

$$|\Psi\rangle_{123} = \frac{1}{2}\Big[ \, |\Psi_-\rangle_{12} \left( -\alpha \, |\mathrm{H}\rangle_3 - \beta \, |\mathrm{V}\rangle_3 \right) \tag{3.3}$$

$$+ \, |\Psi_+\rangle_{12} \left( -\alpha \, |\mathrm{H}\rangle_3 + \beta \, |\mathrm{V}\rangle_3 \right) \tag{3.4}$$

$$+ \, |\Phi_-\rangle_{12} \left( +\beta \, |\mathrm{H}\rangle_3 + \alpha \, |\mathrm{V}\rangle_3 \right) \tag{3.5}$$

$$+ \, |\Phi_+\rangle_{12} \left( +\beta \, |\mathrm{H}\rangle_3 - \alpha \, |\mathrm{V}\rangle_3 \right) \Big] \, . \tag{3.6}$$

It can now be seen that if Alice sends to Bob the result of her measurement Bob can perform a local unitary transform to his qubit which will result in him having the identical state to the one Alice started with. The specific transformations are given in Table 3.1.

**Table 3.1.:** Transform performed by Bob conditional on Alice's measurement.

| Alice's measurement result | Transform performed by Bob |
|:---:|:---:|
| $|\Psi_-\rangle$ | $\hat{\mathbb{1}}$ |
| $|\Psi_+\rangle$ | $\hat{\sigma}_z$ |
| $|\Phi_-\rangle$ | $\hat{\sigma}_x$ |
| $|\Phi_+\rangle$ | $\mathrm{i}\hat{\sigma}_y$ |

The complete teleportation protocol with Victor receiving from Bob the final state to verify the teleportation is shown in Fig. 3.2.

In the work to follow we will note the signal indicating which measurement result Alice obtained that is sent to Bob as the *classical channel* and the entangled particles as the *quantum channel*. With this nomenclature it is said that a quantum state is sent via dual quantum and classical channels, indeed in the original paper Asher Peres (one of the co-authors) wanted to say that the quantum state was disembodied [into it's classical and quantum parts] then reincarnated [38].

### 3.1.2. Higher dimensional teleportation

The N-dimensional generalisation of this protocol, also given in the seminal paper of Bennett et. al. [5], follows exactly the same principles as the two dimensional case. Alice and Bob share a maximally entangled pair and in addition Alice is given the unknown quantum state. A suitable entangled state is

$$|\psi\rangle_{23} = \frac{1}{\sqrt{N}} \sum_{j=0}^{N-1} |j\rangle \, |j\rangle \, . \tag{3.7}$$

Alice then performs a joint measurement on her two particles (in a maximally entangled basis) sending the result to Bob. A possible basis for such a measurement is
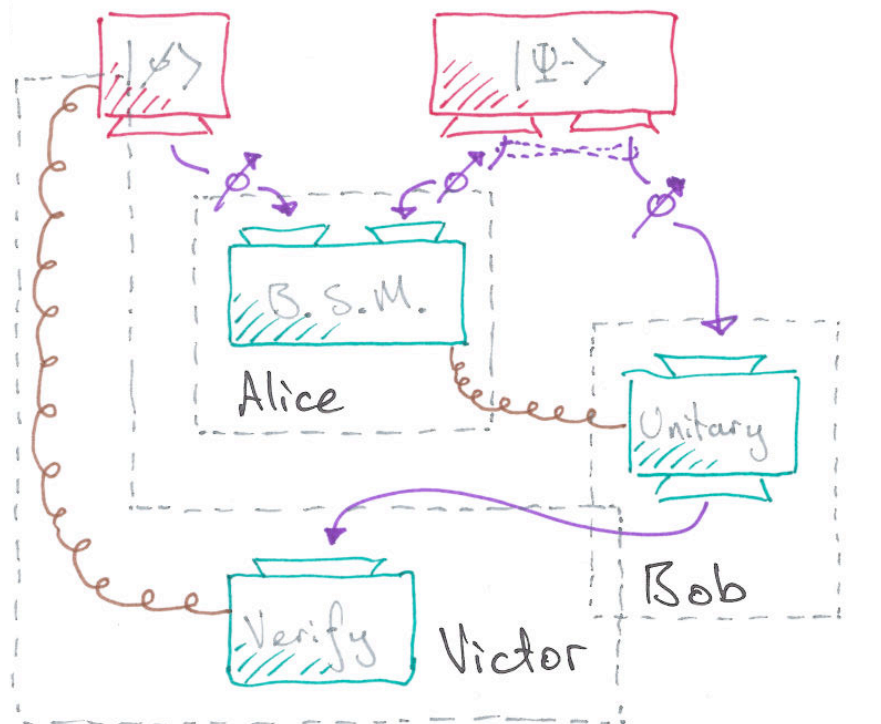
**Figure 3.2.:** Schematic representation of the teleportation protocol with verification. The input state and the entanglement resource are created and sent to their respective parties then Alice performs a Bell state measurement on her two particles. Bob then performs a unitary operation on his particle conditional on the measurement result of Alice. Finally Victor checks the output state against the input state to verify the teleportation protocol.

$$|\psi_{nm}\rangle_{12} = \frac{1}{\sqrt{N}} \sum_{j=0}^{N-1} e^{2\pi ijn/N} |j\rangle |(j+m) \bmod N\rangle \ . \tag{3.8}$$

Finally Bob makes a transform on his particle conditional on the result of Alice's measurement transforming it to the desired state. If the entangled state initially shared by Alice and Bob is as given in Eq. 3.7 and the measurement basis as in Eq. 3.8 then the transform that Bob must apply is given by

$$U_{nm} = \sum_{j=0}^{N-1} e^{2\pi ijn/N} |j\rangle \langle (j+m) \bmod N| \ . \tag{3.9}$$

Some important features of these protocols should be noted. First because of the nature of the measurement that Alice performs she gains no information about the unknown quantum state. Secondly before Bob receives the message telling him which unitary transform to perform he can gain no information at all about the state being teleported. This can be seen to be a consequence of the fact that the completely mixed state of the two particles that Alice receives is an equal superposition of all the maximally entangled states that form the basis for her joint measurement. Thus the particle sent to Bob is equally likely to be in any of it's possible states hence no information is sent faster than Alice's message about the measurement result, which is bound by the speed of light showing that the scheme is consistent with relativistic theories.

### 3.1.3. Generalisations

As noted in the original paper of Bennett et. al. [5] the teleportation protocol is a linear process and thus entanglement between the particle to be teleported and another particle would be preserved. Therefore teleportation of one of a system of entangled particles is a form of entanglement swapping [49, 5]. Also one can imagine carrying out two teleportation experiments, thus teleporting two quantum states, two qubits say. As stated entanglement of those qubits to other systems would be preserved, and thus if the two qubits that were teleported were entangled with one another, then in this protocol entanglement would be teleported. N-state teleportation was generalised to infinite dimensional systems by Vaidman in 1994 [47]. Later Braunstein and Kimble [10] gave a specific protocol for the teleportation of an electric field mode. Such infinite dimensional protocols still follow the same procedure as the original qubit teleportation protocol, with entanglement preparation, measurement in a maximally entangled basis, transmission of the measurement result and finally some operation by Bob dependent upon the message from Alice.

## 3.2. Previous teleportation experiments

### 3.2.1. Bouwmeester et. al., Innsbruck, 1997

Quantum state teleportation was first experimentally demonstrated in 1997 by Bouwmeester et. al. in Innsbruck [8]. The quantum state that was teleported was the spin state of a photon i.e. a single qubit. A visibility of 0.70(3) was measured for input states of $|H\rangle$ and $|D\rangle$.

**Entanglement and input preparation.** In the experiment type II non-collinear spontaneous parametric down-conversion (SPDC) was used as a source of polarisation entangled photon pairs, see Chap. 4.2 for further details. A successful four-fold coincidence detection (at detectors D1 to D4(a or b)) implied the creation of two separate pairs, one pair in spatial modes 1 and 2 and the other in modes 3 and 4. The experimental setup and detector nomenclature used is shown in Fig. 3.3 below.
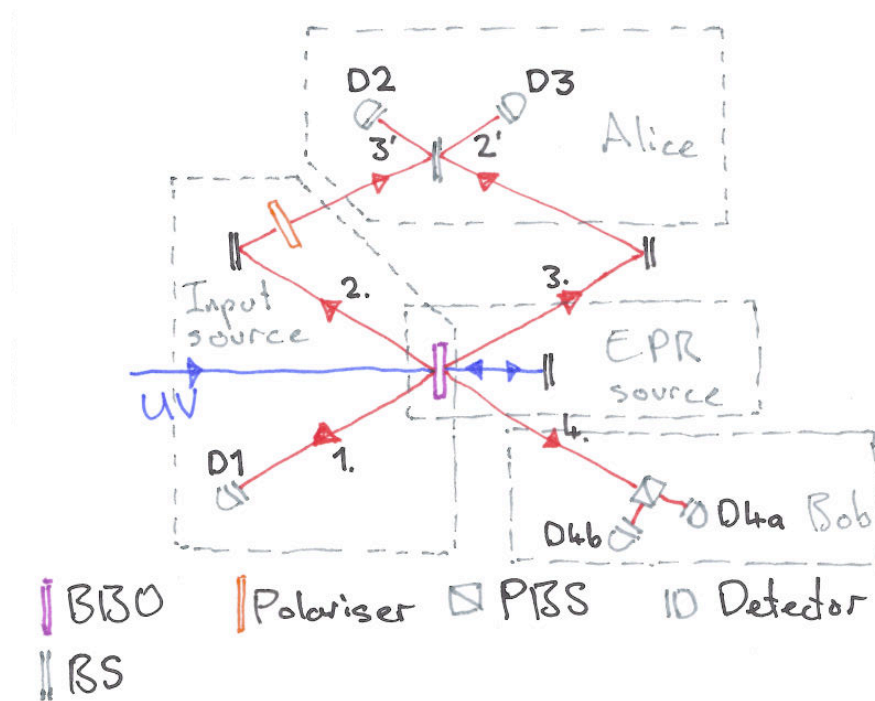


**Figure 3.3.:** Setup used in the Innsbruck experiment. UV pulse pumps a BBO crystal producing two polarisation entangled photon pairs, one is used as the entanglement resource and the other to create the input qubit. Alice utilises a BS and detection to perform a partial Bell state measure and Bob/Victor verify the teleportation.

The entangled spin states of photons in spatial modes 1 and 2 (we will denote these qubits 1 and 2) are used to create the input state. We will call this photon pair the left moving pair. Qubit 1 is detected at detector 1 (D1 in Fig. 3.3) leaving qubit 2 in a Fock state. A polariser in spatial mode 2 is used to prepare

the polarisation of qubit 2, thus allowing (with the use of a wave plate) for input of an arbitrary unknown (to Alice) qubit. This is noted as the Input source and the actions would be completed by Victor. Following the nomenclature above, qubits 3 and 4 form the entanglement resource used as the quantum channel for teleportation. Again following above, this will be called the right moving pair. Qubit 3 is sent to Alice and qubit 4 to Bob.

**Bell state measurement.** The Bell state measurement of Alice on qubits 2 and 3 is realised with a beamsplitter (BS) and two detectors. It can be seen from the four Bell states (Eqs. 2.12 and 2.13) that only the singlet state is spatially anti-symmetric. Thus, as the BS conserves the overall symmetry of the state, the singlet state will be deterministically split with one particle travelling into spatial mode 2′ and the other into 3′, while the other three Bell states (which are spatially symmetric) will bunch such that both photons move into spatial modes 2′ or 3′. Such fourth order wavefunction interference was first noted by Hong, Ou and Mandel in 1987 [20]. It is also noted that for such interference the two wavefunctions must perfectly overlap on the beamsplitter. This was achieved by filtering the photons with 4 nm interference filters and by fine tuning the position of mirror M1. In this manner a partial Bell state measure is made, as coincidence detection between detectors D2 and D3 detects the singlet state. The other three states simply cannot be distinguished.

**Classical signal and unitary transformation.** The classical message sent from Alice to Bob is thus simply to note when a singlet state has been recorded. The unitary operation that Bob must perform in this case is unity, thus he simply forwards his photon on to Victor who verifies the teleportation. In addition he only ever performs this single transformation thus he does not need to actively switch the setup during the experimental run. This measurement of the final state is completed using a polarising beam splitter (PBS) and presumably wave plates to rotate into the basis in which the input state would give 100% contrast between measurements (for example given an input state of $|H\rangle$ the measurement basis would be H/V) followed by detectors at the two PBS outputs.

As mentioned above the visibility, which is defined as

$$V = \frac{\text{True} - \text{Err}}{\text{True} + \text{Err}} \, , \tag{3.10}$$

where True (Err) are the counts of the correct results (incorrect results or errors), for the inputs states of $|H\rangle$ and $|D\rangle$ was 0.70(3). In addition to these four-fold coincidence measurements a number of three-fold coincidence measurements were made. The three-fold coincidences were measured between detectors D2, D3 and D4a or D4b.

Two right moving pairs or one right moving and one left moving pair are created with roughly equal probability. Although two right moving pairs can lead to a three-fold coincidence, qubit 4 is completely un-correlated with the input state. By blocking mode 2 the relative counts of this double right moving pair emission

could be calculated and using this the results were adjusted for this error. The corrected visibilities for the various input states were as follows: $|H\rangle$, 0.66(2); $|V\rangle$, 0.61(2); $|D\rangle$, 0.63(2); $|A\rangle$, 0.64(2); and a circular polarisation state, 0.57(2). In a classical scheme the maximal teleportation visibility averaged over all bases would be[1] 1/3.

It has been noted by Braunstein and Kimble, and later by Kok and Braunstein, that, given the relatively low channel efficiency to Bob, this teleportation protocol is only successful in beating the classical limit if the teleportation is interpreted as post-selected or if we only count polarisation states as errors or correct results [9, 25]. Although all of the photons that arrive at Bob are (to the experimentally measured value) in the same state as the photon to be teleported it is not known when a vacuum state arrives at Bob or when an actual photon does. Thus if the visibility is calculated before the measurement of the photon at Bob/Victor and vacuum states are included as errors then the contribution of the three-fold coincidences at D1, D2 and D3 along with the loss of qubit 4 (due to imperfections in the channel to Bob) would lower the visibility below the classical limit. Bouwmeester et. al. in reply to these arguments write that the absence of a photon does not imply a reduction in fidelity, only in efficiency [7]. In the literature teleportation with low efficiency in the link to Bob is simply called teleportation, whereas teleportation where the efficiency of the quantum channel to Bob is high enough that the teleportation visibilities including the vacuum state contribution surpasses the classical limit is generally called *deterministic* teleportation.

## 3.2.2. Boschi et. al., Rome, 1998

In the second experiment on quantum state teleportation by Boschi et. al. again a single qubit, realised as the polarisation state of a photon, was teleported, however the entanglement resource that was shared between Alice and Bob was a path entangled state of a pair of photons [6]. This allowed the teleportation protocol to utilise only two photons and additionally to realise a Bell state measure that could differentiate all four Bell states however the state that was teleported could not be unknown. That is to say the state of the qubit that is teleported would have to be known by Alice (or more precisely the person who adjusts the Fresnel rhomb polarisation rotators (FRP) noted as 'input source' in Fig. 3.4). For this reason we denote teleportation experiments of this nature *teleprepreparation*. Shown below (Fig. 3.4) is a diagram of the experimental setup.

**Entanglement and input preparation.** As in the work of Bouwmeester et. al. type II SPDC was used to create polarisation entanglement. Thus the state

---

[1]This can be seen as in one basis the visibility could be 1, by simple measurement and preparation, however due to perfect measurement in that basis no information would be available about the other two bases and thus visibilities in these bases would be 0, averaging then gives the value of 1/3
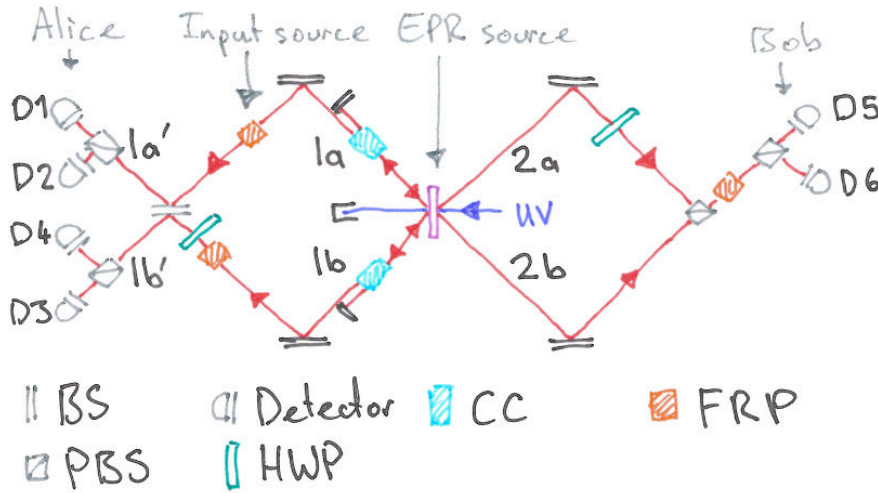
**Figure 3.4.:** Setup used in Rome scheme. A polarisation entangled photon pair is created through parametric down-conversion. This entanglement is then converted to path entanglement with two CC's. The input state is given using FRP's in each spatial mode of the left moving photon. Alice performs a complete Bell state measure utilising a beam splitter and detection. Bob/Victor verify the teleportation results.

directly after successful generation of an entangled pair was

$$|\Psi\rangle_{12} = \frac{1}{\sqrt{2}} \big( |H\rangle_{a1} |V\rangle_{b1} + |V\rangle_{a1} |H\rangle_{b1} \big) \, , \tag{3.11}$$

where a and b denote the 'above' and 'below' spatial modes in Fig. 3.4 and 1 and, later, 2 denote the left and right spatial modes respectively. Next the polarisation entanglement is transformed into path entanglement. Calcite crystals (CC) in paths $1a$ and $1b$ were used to separate the horizontal and vertical polarisations with horizontal being reflected at the mirror following the CCs. Thus the maximally path entangled state after this action is

$$|\Psi\rangle_{12} = \frac{1}{\sqrt{2}} \big( |a\rangle_1 |a\rangle_2 + |b\rangle_1 |b\rangle_2 \big) |V\rangle_1 |H\rangle_2 \, , \tag{3.12}$$

where we have written the above/below entangled spatial mode out explicitly. In Eq. 3.12 we also see that the state is now separable with regards to polarisation. The final step in the preparation of the teleportation of the quantum state is to set the polarisation state to be teleported. This is done with quarter-wave plates and/or FRP acting identically on paths $1a$ and $1b$. Thus any arbitrary polarisation may be given to the input qubit.

**Bell state measurement.** The two qubits that are jointly measured in this measurement are the path and polarisation degrees of freedom of the left photon, photon 1. Following exactly the work of Boschi et. al. a maximally entangled basis is defined as

$$|c_{\pm}\rangle = \frac{1}{\sqrt{2}} \big( |a\rangle_1 |V\rangle_1 \pm |b\rangle_1 |H\rangle_1 \big) \tag{3.13}$$

$$|d_{\pm}\rangle = \frac{1}{\sqrt{2}} \big( |a\rangle_1 |H\rangle_1 \pm |b\rangle_1 |V\rangle_1 \big) . \tag{3.14}$$

A half-wave plate is used to rotate the polarisation of the spatial mode $b$ such that $|H\rangle \rightarrow |V\rangle$ and $|V\rangle \rightarrow -|H\rangle$ allowing spatial mode identification through polarisation. The position of the BS is also adjusted such that states with zero phase between the paths $a$ and $b$ (i.e. states of the form $|a\rangle + |b\rangle$) travel into mode $a'$ and states with 180 deg. phase between paths $a$ and $b$ (i.e. $|a\rangle - |b\rangle$) travel into mode $b'$ thus identifying the phase between the spatial modes. Hence the four detectors each correspond to detection of one of the four states given in Eqs. 3.13 and 3.14, namely D1 $\Rightarrow |d_-\rangle$, D2 $\Rightarrow |c_+\rangle$, D3 $\Rightarrow |d_+\rangle$ and D4 $\Rightarrow |c_-\rangle$.

**Classical signal and unitary transformation.** It is then imaginable that Alice could relay the result of her measurement to Bob, who would perform one of four distinct unitary operations that would transform his (spatial) qubit to the original state of the input (polarisation) qubit. This teleported qubit could of course be realised in polarisation or spatial mode.

In the experiment no such transformation was made rather a half-wave plate in path $2a$ and a polarising beam splitter (PBS) to combine the two spatial modes were used to convert the spatial qubit to a polarisation qubit. Then another Fresnel rhomb device and a quarter-wave plate were used in conjunction with a PBS and two single photon counters to measure the contrast of the photon count rate in the basis in which the input polarisation qubit would give unit visibility. In their work Boschi et. al. show the classical limit for *fidelity*, where only two orthogonal bases are measured, to be 3/4. The fidelity is defined as

$$F \equiv \text{Tr}\big(\hat{\rho}_{exp} |\psi_{in}\rangle \langle \psi_{in}|\big) , \tag{3.15}$$

where $|\psi_{in}\rangle$ is the state to be measured and $\hat{\rho}_{exp}$ is the measured teleported state. Briefly, this limit could be realised as the measurement of one basis and then classical preparation of that state, which would have a maximum fidelity of 1 in the measured basis and 0.5 in the other, orthogonal, bases, thus giving on average a fidelity (over two bases) of 3/4. Boschi et. al. then measure this fidelity for their scheme averaging over three measurements in the H/V and D/A bases (0, 120 and 240 deg.) and also averaging over all Bell states with the result F = 0.853(12), some 8 standard deviations above the classical limit. They also show that circular polarisation states may be teleported with their setup.

The implementation of this scheme raises the question of what is an unknown quantum state. Peres interestingly notes that the very name 'unknown quantum state' is a contradiction in terms [38], indicating the difficulty in interpreting exactly the language of quantum mechanics. We will attempt to avoid such

discussions here, but there is a difference between what Boschi et. al. call an unknown quantum state and what Bouwmeester et. al. call an unknown quantum state. In the Bouwmeester experiment the input is the polarisation state of a photon in a Fock state. This photon can in principle come from any 'outside' source, and thus could of course be entangled with another system. Thus it is certainly unknown to Alice and Bob, but also could be unknown in the sense that it is part of a maximally entangled state. However in the scheme of Boschi et. al. they note that this work is the same up to a local unitary transformation as the original scheme proposed by Bennett et. al. But the transform, which is the transfer of the quantum state from an 'outside' particle onto the polarisation degree of freedom of photon 1 is only 'local' in the sense that it is only performed at Alice, but it is not localised to one point in space as it necessarily must be performed on two separate spatial modes. Thus, for example, in this scheme an entangled particle could not be used as the unknown quantum state. It is also noted that in the work of Jin et. al. [22], presented below, they also claim that the scheme is the same as the original scheme up to a local unitary transform, but here again the word local must be taken to mean local to Alice.

### 3.2.3. Other schemes of particular interest

The two schemes given above illustrate the first two realisations of quantum teleportation and also illustrate two possible realisations of two-dimensional quantum state (i.e. qubit) teleportation in photonic systems and thus are of particular interest to this work. However many other schemes have been realised.

In 1998 Furusawa et. al. realised the deterministic teleportation of an infinitely dimensional quantum system, namely an optical coherent state [18] following the proposal of Braunstein and Kimble [10]. The fidelity of the teleported photonic coherent state with respect to the input coherent state was 0.58(2), in excess of the maximum obtainable fidelity of 0.5 for coherent states using classical schemes.

Teleportation schemes have also been completed in other mediums. The first such experiment, by Nielsen et. al. (1998) demonstrated teleportation using liquid-state nuclear magnetic resonance [36]. A qubit realised in a carbon atom which itself was part of a trichloroethylene molecule was teleported to a hydrogen atom in the same molecule. In the experiment they use entanglement fidelity as a figure of merit for teleportation[2] and measure a (highest) value of roughly 0.88(5), see [36] for a figure showing this value and it's temporal dependence (as decay times are of central importance to this experiment). Two experiments in trapped ions in 2004 showed teleportation with fidelities better than classical schemes. In the experiment by Barrett et. al. using Beryllium ions ($^9Be^+$) a fidelity of 0.78(2) is

---

[2]Entanglement fidelity ranges from 0-1 with 1 representing perfect teleportation and 0.25 representing a random state as output. The best classical scheme would give a value of 0.5 [36]

demonstrated [3] and Riebe et. al. (utilising Calcium ions ($^{40}Ca^+$)) show a fidelity of 0.75(3) [39].

Quantum state teleportation was also demonstrated between two different systems, namely a coherent state of light was teleported to an atomic ensemble [43]. The work, by Sherson et. al., is of particular interest as it demonstrates the ability to change 'flying' quantum states to 'stationary' quantum states, which is seen as an important tool in the creation of a quantum computational network [14]. The experiment demonstrated fidelities of 0.58(2) and 0.60(2) for coherent states with mean photon number of 20 and 5 respectively.

Entanglement swapping, which as stated in Chapter 3.1.3 is a natural extension of the teleportation protocol, was first experimentally realised in 1998 by Pan et. al. [37]. In their work two entangled pairs of qubits were created, the first of which we shall denote qubits 1 and 2 and the second 3 and 4. The qubits were realised as the spin states of photons. Then using the same Bell state analysis as described for the teleportation experiment of Boumeester et. at. [8] the entanglement was swapped from between qubits 1 and 2 and qubits 3 and 4 to between qubits 1 and 3 and qubits 2 and 4. Later the non-local nature of this protocol was demonstrated, through the violation of a Bell inequality, by Jennewein et. al. [21].

All of the experiments given above were carried out in a laboratory setting, however some experiments have demonstrated teleportation over much longer distances. The first long distance experiment was carried out by Marcikic et. al. over a distance of 55 m from one laboratory to another using optical fiber (of length 2 km) [34]. Ursin et. al. then teleported a photonic based qubit 600 m under the Danube river [45]. The quantum channel used to transmit the qubit was, as in the Marcikic experiment, a fiber optic cable. The scheme used was very similar to that of Bouwmeester et. al. [8] (see Chap. 3.2.1) although a more complete Bell state measure was made which allowed for identification of two of the four Bell states, see Chap. 4.4. This information (about which Bell state was measured) was then sent using a radio frequency classical channel to Bob who performed the correct unitary operation dependent upon the signal from Alice. The measured state fidelity over three orthogonal bases was 0.86. Recently (2010), Jin et. al. reported a long distance photonic telepreparation experiment [22]. The experiment followed the scheme of Boschi et. al. [6] (see Chap. 3.2.2) however it also explicitly implemented the classical channel and unitary operation at Bob. Also the path length between the two paths of the single qubit that is sent to Alice was actively controlled using piezoceramic translation stage controlled by a secondary laser in the beam path. The total distance of the free space link was 16 km and the measured state fidelity of the teleported qubit was 0.89.

# 4. Experimental methods

In this chapter we will discuss the setup that has been constructed in Vienna for the completion of the teleportation experiment. It is planned that we will partially deconstruct this setup and then move it to La Palma for the final experiment. First a brief outline of the requirement for the experiment will be given then an overview of the entire setup and finally more detailed discussions of the sections of particular interest.

As stated, the end goal of this experiment is quantum state teleportation between La Palma and Tenerife, two of the Canary Islands, separated by 144 km. It is important to understand the requirements placed on the setup by the link. The link is a free space optical link. The receiving telescope employed is the optical ground station (OGS) of ESA, a 1.016 m diameter reflecting telescope. The sending telescope is a 7 cm diameter lens mounted on a breadboard which is dynamically aligned with a tracking system previously used in this group. For details on the telescopes and the tracking system see [46]. Due to atmospheric turbulences the link fluctuates very heavily on time scales less than around five seconds[19]. As during the day high dark counts (from the ambient light) are encountered we can only use this link during the night and thus we are restricted to around six hours of useful time each day if weather conditions are good. When the weather conditions become poor then we simply cannot use the link for that time. Most importantly the time averaged attenuation (to average over the aforementioned atmospheric turbulence) of the link is roughly 30 dB, in good conditions. Also polarisation over the link has been found to be stable in previous experiments.

Following from the nature of the link (and the resources available) the following requirements are placed on the setup:

- Qubits are to be realised as the polarisation states of photons.

- The source must be very bright such that we still have a high enough photon rate after the 30 dB attenuation to show teleportation above the classical limit. Thus the approximate successful teleportation rate should be in the region of tenths of Hertz (or greater).

- The source must be stable over the time span of at least an hour, and ideally for an entire night's data collection on the Canary Islands.

- The teleportation visibility must be suitably high, as low visibility is both inherently undesirable and also would require longer integration times to give the same violation of the classical limit.

- We must be able to disassemble the setup then transport it to La Palma then reassemble it in a reasonable time scale and without loss of the quality of the setup.

- The setup must be fairly robust as the conditions in the lab at La Palma will not be as good as we have in a laboratory.

With these factors in mind we use a setup similar to that of Bennett et. al. [5] (see Chap. 3.2.1) however the setups differ in a number of ways. Most notably a more complete Bell state measurement is implemented, the Fock state source was changed from type II non-collinear to type II collinear spontaneous parametric down-conversion and the possibility of using a weak coherent pulse directly from the laser was added. In addition the setup is built on a number of breadboard so that all of the optical mounts could be shipped still attached to their respective breadboard making the reconstruction on the Canary Islands much simpler.

## 4.1. Overview

Figure 4.1 shows the setup used in this work, unessential components are not included (for a complete diagram see App. A.2). The setup is broken down into six major sections (and are labelled as such Fig. 4.1) which we now discuss in turn.

**1. UV preparation:** We use a mode-locked Titanium-Sapphire laser[1] which produced a pulsed beam with repetition rate of 80 MHz, a pulse width of 180 fs, a central wavelength of 808 nm and approximately 4 W average power. This light is first passed through a type-I cut Beta-Barium Borate (BBO) crystal up-converting the light to 404 nm (UV). After up-conversion eight dichroic mirrors (represented by a single mirror in Fig. 4.1) which reflect UV and transmit 808 nm light remove the remaining 808 nm light from the beam. We are left with a beam of approximately 1.4 W power at 404 nm that is polarised vertically.

**2. WPC input:** The 808 nm light that passes through the first of these dichroic mirrors is used as the weak coherent pulse (WCP) input. As this light is just the light that was not up-converted the WCP input is simply strongly attenuated light directly from the laser. A delay stage, beam expander tube and a number of polarisers are used to control the timing, intensity and polarisation of the pulse.

**3. EPR source:** The 1.4 W of 404 nm light from the UV preparation is focused onto a type-II cut BBO producing photon pairs entangled in wavelength, time and polarisation in separate spatial modes via non-collinear spontaneous parametric down-conversion (SPDC). The polarisation state of the photon pairs is a $|\Psi-\rangle$ state. The photons are then coupled into single mode fibers and one is sent to

---

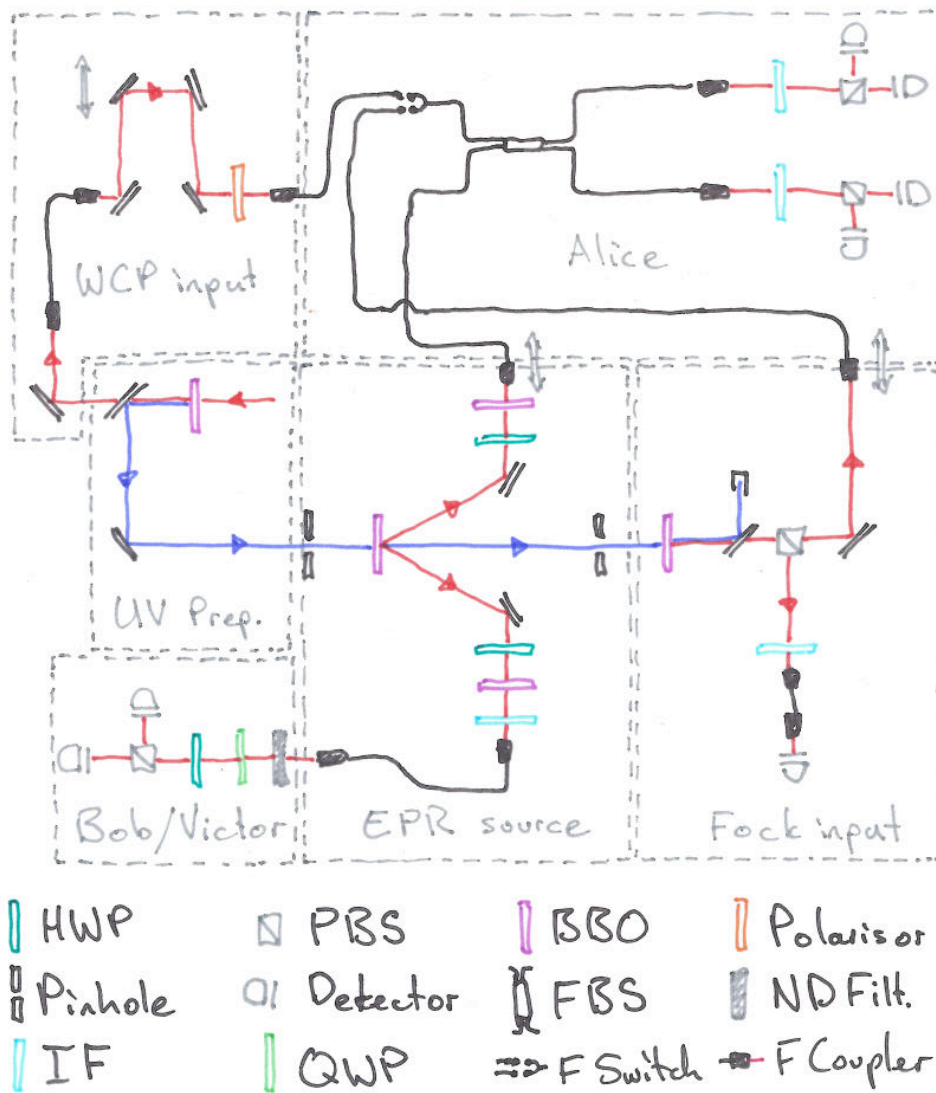[1]A 'Chameleon Ultra II' made by Coherent.

**Figure 4.1.:** Setup built in laboratory for long distance teleportation. UV light (blue lines) pumps successively two BBO's, producing two entangled photon pairs (red lines). The first pair is used as the entanglement resource and the second as a possible input qubit realised as the spin state of a photon in a Fock state. Additionally strongly attenuated laser light is used as an alternate input source as the polarisation state of light in a coherent state. Alice performs her Bell state measurement with a BS and four detectors. Bob/Victor verifies the teleportation. Legend: HWP - half-wave plate, PBS - polarising beamsplitter, BBO - beta-barium borate, FBS - fiber beamsplitter, ND Filt. - neutral density filter, IF - interference filter, QWP - quarter-wave plate, F Switch - fiber switch, F Coupler - fiber coupler.

Alice and the other to Bob. A pinhole is used before this BBO to increase the coupling efficiency.

**4. Fock input:** The remaining UV beam that passed through the BBO of the EPR source, which has approximately the same power as before the BBO (due to the very low efficiency of the down-conversion process) is first collimated then focused onto a second type-II cut BBO. At this BBO we use collinear SPDC, thus the entangled photon pairs are produced in the same spatial mode (see Chap. 4.2). A polarising beam splitter (PBS) is then used to separate the horizontal and vertical polarisations. Both photons are coupled into single mode fibers and the vertically polarised photon is detected heralding the presence of the horizontally polarised photon.

**5. Alice:** A photon from either the Fock Input or the WCP input is sent to Alice along with one of the two from the EPR source. The Bell state measure is made by using a variable fiber beamsplitter (FBS), with the splitting ratio set such that the reflection is 0.5, followed by measurement of the photonic polarisation states. This Bell state measure is not fully efficient, however it can determine the $|\Psi\pm\rangle$ Bell states.

**6. Bob/Victor:** As we are yet to implement the classical channel Bob/Victor simply measures the polarisation of the photon he receives in the appropriate basis.

## 4.2. Photonic conversion and entanglement preparation

Photonic systems have many advantages in quantum computational tasks, these generally stem from the lack of interactions between photons and other systems. Because of this generating interactions between photons, and thus generating entanglement, is particularly difficult. For a recent comparison of various systems for quantum computation see [29]. In this work we use SPDC within BBO crystal to generate single photons and entanglement. SPDC was first observed by Burnham and Weinberg in 1970 [11], later entanglement between the produced photon pairs was demonstrated [1, 44] and in 1995 the technique was used to generate entanglement in the polarisation degree of freedom [27]. Since then a large body of work has been completed in developing these techniques[2] and in addition many theoretical descriptions of the process can be found[3]. Here we will simply consider the topic from an experimental perspective.

---

[2]For a general introduction to coupling efficiency optimisation in type-II non-collinear SPDC see Kurtsiefer et. al. [26]. Ljunggren and Trengner and Lee et. al. discuss focusing of the pump beam [33, 32]. Crystal thickness is discussed by Lee et. al. [31]. Kwon et. al look at the coupling efficiencies for beam-like, collinear and non-collinear situations [28].

[3]Although a number of papers exist on the subject (for example [40]) it is my opinion that many theses cover this topic in a more suitable manner, see [23] for example.

We utilise three photonic conversion processes. Firstly the up-conversion[4], where $|V\rangle_a^{808} |V\rangle_a^{808} \rightarrow |V\rangle_{a'}^{404}$, where $|V\rangle_a^{808}$ means a single vertically polarised photon in spatial mode $a$ with central wavelength 808 nm, we define the extraordinary polarisation as vertical and ordinary as horizontal. Figure 4.2 illustrates the spatial mode nomenclature used here. Secondly type-II non-collinear down-conversion[4] is used for the entanglement resource preparation, where $|V\rangle_a^{404} \rightarrow (|V\rangle_{b'}^{808} |H\rangle_{c'}^{808} + e^{i\phi} |H\rangle_{b'}^{808} |V\rangle_{c'}^{808})/\sqrt{2}$ and finally type-II collinear down-conversion[4] is used to prepare the Fock input state where $|V\rangle_a^{404} \rightarrow |H\rangle_{a'}^{808} |V\rangle_{a'}^{808}$.
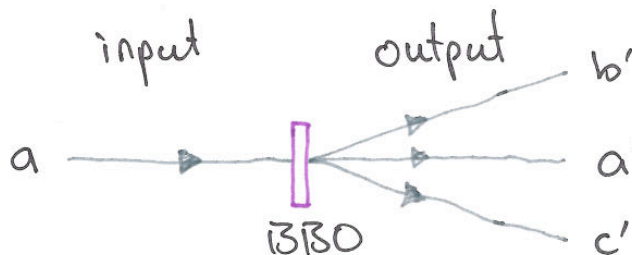


**Figure 4.2.:** Birds-eye view of SPDC showing the spatial mode nomenclature used. Spatial modes $a$ and $a'$ are the input and output beams directly along the optical axis. Modes $b'$ and $c'$ are the spatial modes corresponding to the crossing points in non-collinear down-conversion, these are further illustrated in Fig. 4.3.

The light fields that enter and exit the non-linear crystal must approximately fulfil conservation of energy and momentum. In type-II down-conversion this leads to two emission cones, one horizontally polarised and the other vertically, in which the light may be emitted. As the crystal is tilted, shown in Fig. 4.3, the central paths of these cones, and their spreading changes such that there are three distinct cases within type-II SPDC. The rings shown in Fig. 4.3 are made up of many photon pairs that are correlated to conserve energy and momentum with the entire upper ring consisting of vertically polarised photons and the lower ring of horizontal photons.

In Fig. 4.3b we see that by collecting photons from the crossing points of the two rings we collect photon pairs with orthogonal polarisation in the H/V basis. This is the non-collinear configuration, and as stated is used at the EPR source. Shown in Fig. 4.1 directly before the down-converted photons are coupled into single mode fiber there is a BBO. The primary purpose of this BBO is to compensate for walkoff effects (see below), however by tilting one of the compensation BBO's

---

[4]In these conversions one photon is converted into a photon pair, or a photon pair is converted into a single photon. Up-conversion is where the photons of the photon pair are of lower energy are converted into a single higher energy photon. Down-conversion is where a higher energy photon is converted into a pair of photons with lower energy. Type-I means that the photon pair has the same polarisation as the single photon whereas type-II is where the photons of the photon pair have orthogonal polarisation. Non-collinear and collinear are shown in Fig. 4.3 and discussed in the main text.

relative to the other (parallel to the optic axis) a phase shift is induced between the two spatial modes as the effective thickness of the BBO is changed. By tuning this phase to 180 deg. we then obtain the desired $|\Psi-\rangle$ state as given in Eq. 2.12.

For the Fock state input source we utilise collinear down-conversion followed by a PBS to separate the photon pair into two distinct spatial modes. Thus no polarisation entanglement is present in the spatially separated state (after the PBS), however the temporal correlation remains and thus we may still herald one of the photons with the measurement of the other. A collinear setup is used as it allows for greater coupling efficiencies due to better quality of the spatial mode (as compared to the non-collinear case). Also because we must verify the teleportation we want a definite polarisation state as an input qubit and by utilising the PBS we get exactly this with (close to) unit efficiency. However if we used a non-collinear setup the state would initially be an indeterminate mixture of H and V, and thus we would have to halve the count rate (i.e. by using a polariser) to obtain a desired state.
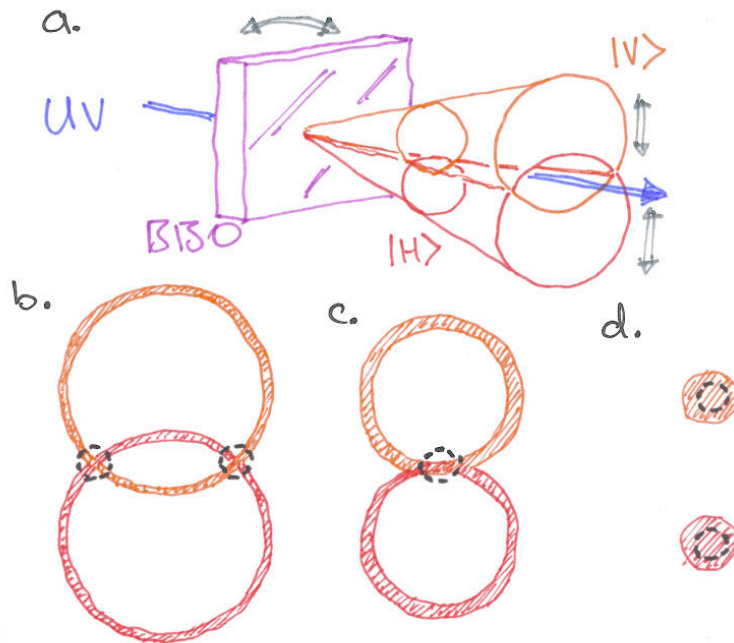


**Figure 4.3.:** Output ring configuration in SPDC. a. Schematic view of non-collinear down-conversion showing down-conversion cones, BBO crystal and UV pump beam. As one tilts the BBO in the direction of the pump beam the cones shrink and expand in diameter. b. Non-collinear down-conversion ring profile. c. Collinear down-conversion ring profile. d. Beam-like down-conversion 'ring' profile. Figure based on work by [23].

After the BBO of the EPR source we place half-wave plates (HWP's) followed by BBO's (see Fig. 4.1) in both of the down-converted modes. As BBO is highly birefringent there is a spatial and temporal displacement induced between the two beam paths (which are orthogonally polarised) as shown in Fig.

4.4. This displacement is both a longitudinal walkoff and a transverse walkoff, we will simply refer to this as a walkoff. By switching the horizontal and vertical polarisations (with HWP's) and passing the beams back through the second compensation BBO's, that are half the thickness of the primary BBO, we may partly compensate for this walkoff effect. Because down-conversion is an approximately spontaneous process the entangled pairs may be produced at any point through the BBO crystal thus this compensation is only perfect for pairs created exactly in the middle of the down-conversion BBO, however on average this compensation helps to remove the spatial and temporal distinguishability (which reduces the entanglement quality) induced by the walkoff.
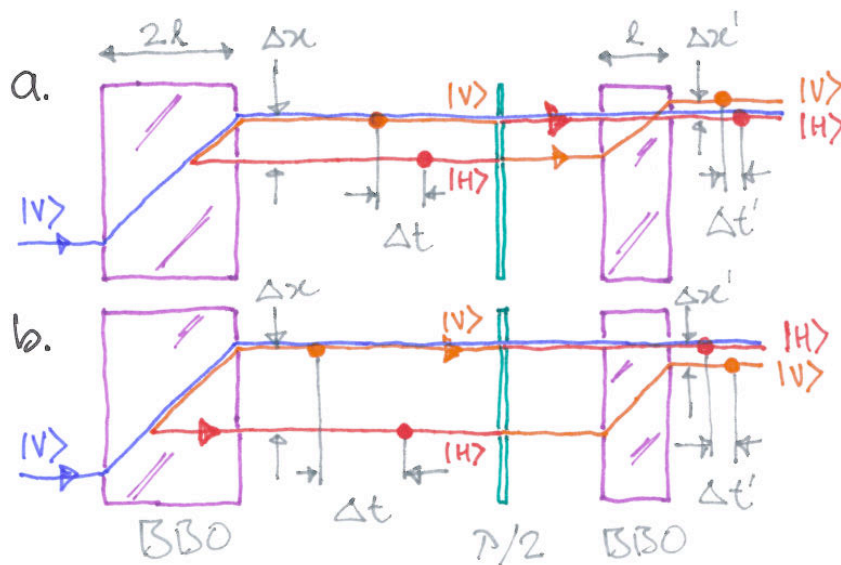


**Figure 4.4.:** A HWP and a second BBO, with half the thickness of the down-conversion BBO, are used to compensate for the walkoff induced by the down-conversion BBO. Figures a and b are two different examples of possible positions of down-conversion and the corresponding effect of the compensation.

In addition to the walkoff, and despite the compensation of the position of the horizontal and vertical spatial modes, the beam profile of the vertical (as horizontal and vertical polarisations are flipped due to the HWP) photons will be elongated into a non Gaussian mode as they are produced over a range of position in the vertical dimension of the crystal. This is a problem firstly as the two modes must be indistinguishable to be entangled, thus imperfect spatial mode overlap reduces the entanglement quality. To remove the spatial distinguishability we couple the light into single mode fibers. This allows us to regain the high quality entanglement, but reduces the counts, and in particular of the vertically polarised photons as the mode overlap of the fiber with the elongated vertically polarised mode is poor.

## 4.3. Efficient coupling

As the pump power, and thus rate of down-conversion pairs, increases so too does the error rate. Thus we are in a situation where there is an intrinsic trade-off between the source signal to noise ratio and the source brightness. To make matters worse, if the coupling of the down-converted pairs into the single mode fibers is well below unity (the coupling in this experiment, is between 0.1 and 0.2), then it is much more likely that higher order emissions will lead to a coincidence measurement than the single pair emission thus with poor coupling the effect of higher order emissions becomes apparent at lower count rates which effectively lowers the count rate at which the source can be used for a given error tolerance level.[5] Thus one of the most important tasks to allow for high count rates while still maintaining high visibility was to improve the coupling efficiency.

In this work we define coupling efficiency as

$$\eta_i = \frac{n_{ij}}{n_j} \, , \tag{4.1}$$

where $n_{ij}$ is the coincidence count rate of the detection of photons from spatial modes $i$ and $j$, where mode $j$ must be the paired mode to $i$. Paired modes are 1 and 2 and modes 3 and 4. $n_j$ is the single count rate of photons from spatial mode $j$. The spatial mode (and detector) nomenclature used here is given in Fig. 4.5. It is noted that defining the coupling efficiency this way is only approximately equivalent to the actual probability that a single photon that is created at the source will be detected at an appropriate detector[6] and also that this efficiency includes the detection efficiency.

### 4.3.1. Lens selection

In short, the aim of coupling is to match the spatial mode created after down-conversion, at both the Fock state input and the EPR source, to the respective spatial modes of the single mode fibers that are used for spatial filtering. Firstly, and most obviously, this is done by aligning the single mode fibers: tuning the distance between the coupling lens and the fiber tip, the direction in which the

---

[5]Imagine a simple case where we want to record a two-fold coincidence from the EPR source and we have a coupling efficiency of 10% in both output spatial modes. If we create a single pair then it has a 1% chance that both are coupled. However with a double pair emission we have a 3.6% chance of collecting one photon in each mode.

[6]This definition is particularly useful as it can be easily obtained in the laboratory and makes intuitive sense. However because of errors from higher order emissions it is slightly misleading. If one imagines a source that produced only very high order emissions then even when the probability of a single photon being detected was low the coupling efficiency could be high. This does not present a great problem here though as the double (and higher order) emission rate is low and also we are more interested in this quantity from a qualitative perspective.
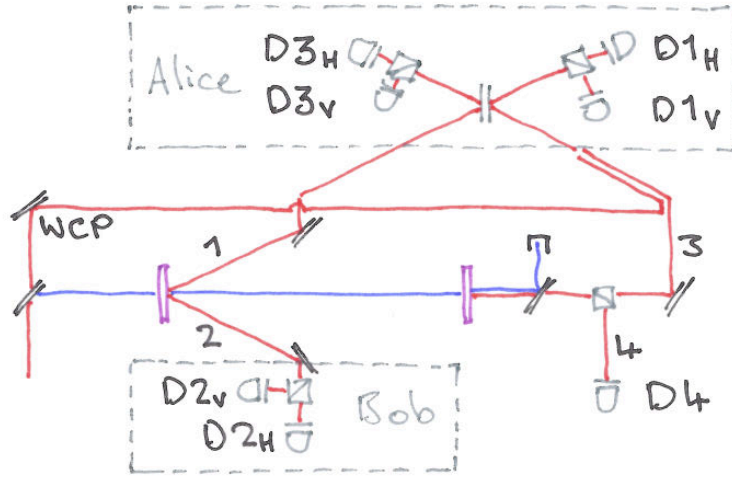
**Figure 4.5.:** Schematic of the setup to show detector and qubit/spatial mode nomenclature.

fibers face and the position of the fibers to the optimal point. Secondly a number of different lens combinations were tried in order to maximise the focusing onto the BBO while still maintaining high quality coupling. As a general rule focusing the UV onto the BBO's with shorter focal lengths lenses will increase the count rates $n_{1,2,3\,\text{and}\,4}$, however the coupling efficiencies, $\eta_{1,2,3\,\text{and}\,4}$, will be decreased (due to worse spatial mode overlap between the beam and the single mode fiber). In Fig. 4.6 we show the lenses used in this experiment.

For the UV preparation a short focal length was chosen in accordance with previous experiments. The actual lens used was most likely a singlet, however, its exact details are not known (it was taken directly from the old setup).

For the EPR source a 150 mm lens was used. From previous experiments it was known that this gives the optimal coupling and count rate. We also tried using a 75 mm lens, however when this was used the count rate was only approximately 10% higher and the coupling was reduced by 30%. The lenses used before all the single mode couplers are 15.4 mm aspheric lenses. These again were known from previous experiments in this group to be optimal for coupling the down-converted light with a 150 mm lens used for focusing onto the BBO (as is the case for this source).

For the Fock state preparation the higher mode quality allowed for the use of a lens with shorter focal length. We use a 75 mm lens, in addition a 100 mm lens and a 50 mm lens were tested. The 100 mm lens gave approximately 10% worse coupling, averaged over $\eta_3$ and $\eta_4$, and 15% worse two-fold count rate ($n_{34}$) in comparison to the case with the 75 mm lens. With the 50 mm lens the coupling was around 20% lower and the count rate 25% lower. In addition to the 15.4 mm aspheric lenses used we tested 8 and 6 mm aspheric lenses for the focusing onto the single mode fiber. Although the overall count rate, that is the single count rates, for all lenses was roughly equal (within 10%) the 8 mm lens gave
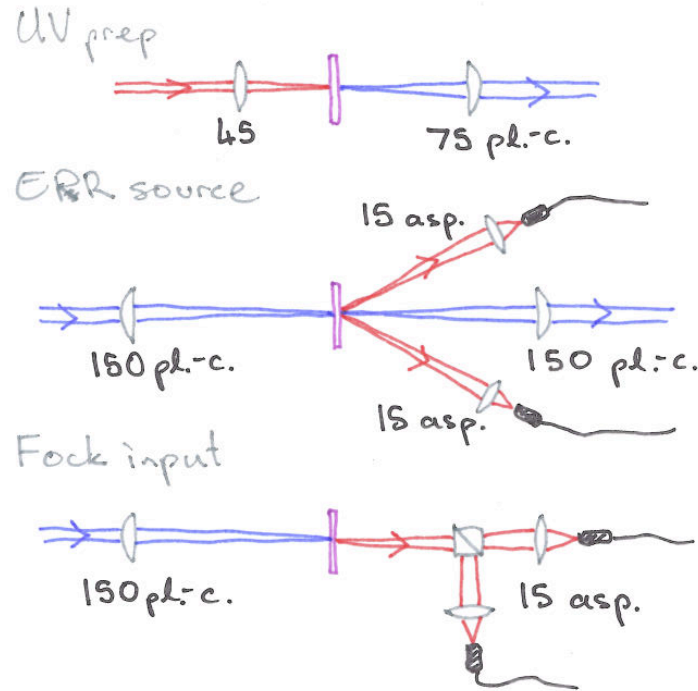
**Figure 4.6.:** Lens configuration used in experiment. pl.-c. is short for plano-convex and asp. is short for aspherical lens. The numbers given are the focal lengths in mm. All lenses were coated with the appropriate anti-reflection coating.

approximately 10% lower coupling than the 15.4 mm lens and the 6 mm lens gave 20% lower coupling than the 15.4 mm lens. These lower coupling efficiencies also meant that the two-fold count rate was lower with lenses with shorter focal lengths, thus we use the 15.4 mm lenses for the Fock state source as well as the EPR source.

## 4.3.2. Use of pinholes

As shown in Fig. 4.1 before both of the down-conversion BBO's we use a pinhole. The use of this pinhole allows two improvements. Firstly we may control the actual count rates at either BBO simply by closing or opening the pinholes, although we can not independently tune the count rates as attenuating the pump before the first BBO also attenuates the pump before the second. The second, and most important, reason for using the pinholes is to increase the coupling efficiency. The beam profile before the pinholes is roughly an elongated Gaussian, with full width half maximum (FWHM) in the horizontal plane of 0.50(5) mm and in the vertical plane 0.67(5) mm. After the pinholes it is assumed that the beam profile follows a Bessel function as would be expected from such an aperture, however no measurements of the beam shape after the pinhole have been completed and this is only a best guess at the beam dynamics. The end effect of the pinhole

is a marked increase in the coupling efficiency with decreasing pinhole diameter. For example for the Fock state source with 88 kHz two-fold rate the coupling of spatial mode 4 (the 'triggering' photon) is 0.140(2), if the pinhole is then closed to give 68 kHz two-folds the coupling is increased to 0.175(2) and further reduction to 33 kHz gives 0.205(2) coupling efficiency. Correspondingly for the EPR source closing the pinhole from approximately 150 kHz two-folds to 80 kHz gives a coupling increase from 0.115(2) to 0.140(2) for spatial mode 1. In both cases the pinhole was paced approximately 6 cm from the lens which focused the pump onto the corresponding BBO.

Qualitatively similar results were also achieved with the previous setup, although a much greater coupling increase was seen. A reduction in two-fold counts for the EPR source of 40 kHz, from 90 kHz to 50 kHz gave an increase of approximately 0.05 in coupling, from 0.12(2) to 0.17(2). Also to get these results two pinholes had to be used at 14 and 45 cm from the focusing lens. On the new source the use of two pinholes was also tried however a second pinhole never gave any improvement and, as stated, the optimal distance from the lens to the first pinhole was some 8 cm displaced.

## 4.4. Bell state measurement

In this work we realise a partial Bell state measurement using a BS, 2PBSs and detection. Figure 4.7 shows the experimental setup used for this measurement. The BS used was actually a variable fiber beam splitter (FBS), however for this experiment the splitting ratio was always set to 50/50.
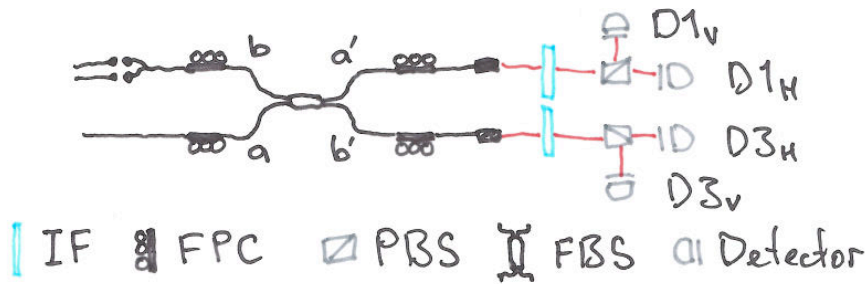


**Figure 4.7.:** Experimental realisation of the Bell state measurement. The input for spatial mode $a$ comes from the EPR source and the input for $b$ from either the WCP input of the Fock input. Legend: IF - interference filter, FPC - fiber polarisation controller, PBS - polarising beamsplitter, FBS - fiber beamsplitter.

The measurement seeks to identify which one of the four Bell states the joint state of the photons from spatial modes $a$ and $b$ (as indicated in Fig. 4.7) are in. The Bell states are given in Eqs. 2.12 and 2.13 and below,

$$|\Psi\pm\rangle = \frac{1}{\sqrt{2}}\big(|\text{H}\rangle_1 |\text{V}\rangle_2 \pm |\text{V}\rangle_1 |\text{H}\rangle_2\big)$$

$$|\Phi\pm\rangle = \frac{1}{\sqrt{2}}\big(|\text{H}\rangle_1 |\text{H}\rangle_2 \pm |\text{V}\rangle_1 |\text{V}\rangle_2\big)\ .$$

The detection setup, consisting of 3 nm interference filters (IF), PBS's and then detection, allows for the measurement of the polarisation and spatial mode of the two photons. In Eqs. 2.12 and 2.13 it can be seen that only $|\Psi-\rangle$ is a spatially antisymmetric state. Detection of both photons in a *single* 'output' spatial mode ($a'$ or $b'$) implies a spatially symmetric state, thus the detection of one photon in *each* of the two spatial modes is only possible if the two photons were originally in the $|\Psi-\rangle$ state. In addition we see that the $|\Psi\pm\rangle$ states have orthogonal polarisation, hence detection of two orthogonal polarisations implies either $|\Psi\pm\rangle$. Thus we have the following:

- Coincidence between
    D1$_H$ and D3$_V$ $\Rightarrow |\Psi-\rangle$, or
    D1$_V$ and D3$_H$ $\Rightarrow |\Psi-\rangle$.

- Coincidence between
    D1$_H$ and D1$_V$ $\Rightarrow |\Psi+\rangle$, or
    D3$_H$ and D3$_V$ $\Rightarrow |\Psi+\rangle$.

To distinguish the two $|\Phi\pm\rangle$ states from one another it is possible to utilise photon number detection, as in [30], however such a setup with our current detectors would reduce the count rates achievable due it's its probabilistic nature. In our setup $|\Phi\pm\rangle$ both result in both photons being detected by a single detector and cannot be distinguished. The effect is that the maximum efficiency with which we can teleport is reduced by half as we must simply disregard these cases. It is noted however that the maximum teleportation visibility is not effected, as the teleportation visibility measures how faithful the final state at Bob is with respect to the initial state given to Alice.

The fourth-order wavefunction interference that is used here was first demonstrated by Hong, Ou and Mandel for symmetric states [20] and is generally referred to as Hong Ou Mandel (HOM) interference. The technique requires that the two photons arrive indistinguishably at the beamsplitter. It can be seen above that the symmetry of the state is of central importance, and thus equally the Bosonic nature of the overall state in centrally important. The two photons are confined to single mode fibers and thus as they overlap upon the FBS they become spatially indistinguishable. To insure that the photons also overlap temporarily we adjust delays that sit before all of the inputs to the FBS. The full details of the technique used to find this delay are given in App. A.1. In addition to fine tuning the temporal delay we also use 3 nm filters before detection.

These spectrally narrow filters broaden in time the wavepacket of the photons, thus broadening the region of effective HOM interference. This serves to increase the probability of successful HOM interference (and equally the measured HOM visibility).

# 5. Results

In this chapter we will present the results of the characterisation of the source. It is noted that all of the results presented here are completed in the laboratory. Where we note attenuation, this refers to the strength of a neutral density (ND) filter, or a number of filters, placed before Bob's measurement module, as shown in Fig. 4.1. All error values given are based on Poissonian statistics.

The major result of this work is the successful teleportation with the WCP input and the Fock input at 31 dB attenuation. Table 5.1 gives the results with the WCP and Table 5.2 gives the corresponding results with the Fock input.

**Table 5.1.:** Results for teleportation using the WCP with 31 dB attenuation. The experiments were carried out in April, 2010. The integration time is 3 hrs, $n_{12} = 41$ kHz, $n_{\mathrm{WCP}} = 2$ MHz and averaged over the runs $\eta_1 = 0.160$, $\eta_2 = 0.138$, the total dark counts at Bob's station are 580 Hz (180 Hz on D2$_H$ and 400 Hz on D2$_V$) and the entanglement had SNR 48:1 in the D/A basis. See Ch. 4.3 for the definition of the notation $n_{ij}$, detector nomenclature is given in Fig. 4.5 and visibility is defined in Ch. 3.2.1. The classical violation number of standard deviations (std.) of error that the measured results are above the best possible classical scheme (that measures each basis equally).

| Input state | Teleportation visibility | Classical violation (std.) |
|:-----------:|:------------------------:|:--------------------------:|
| H | 0.858  (7) | 73.4 |
| D | 0.685  (9) | 39.8 |
| R | 0.701 (10) | 37.4 |
| A | 0.703 (10) | 38.3 |

It can be seen from Tables 5.1 and 5.2 that with attenuation of 31 dB we can successfully demonstrate high quality teleportation, that is teleportation with high visibility and far beyond the best possible classical scheme.

**Using different pulses of the laser**

In this work the EPR pair comes from the same pulse as the input photon (either as a WCP or a Fock state). Although this presents no real problem we were interested to see if we could use inputs from two different laser pulses. Specifically we delayed the WCP input by 25 ns so that the EPR source photon pair was generated in a pulse of the laser *two pulses after* the pulse from which the WCP input came. It was found that this severely reduced the teleportation visibility

**Table 5.2.:** Results for teleportation using the Fock state input with 31 dB attenuation. The experiments were carried out in April, 2010. The integration time is 4 hrs, $n_{12} = 41$ kHz, $n_{34} = 118$ kHz and averaged over the runs $\eta_1 = 0.152$, $\eta_2 = 0.120$, $\eta_3 = 0.102$, $\eta_4 = 0.180$, the total dark counts at Bob's station are 580 Hz (180 Hz on D2$_H$ and 400 Hz on D2$_V$) and the entanglement had SNR 21:1 in the D/A basis.

| Input state | Teleportation visibility | Classical violation (std.) |
|:---:|:---:|:---:|
| H | 0.902 (15) | 37.2 |
| D | 0.749 (22) | 18.7 |
| R | 0.745 (22) | 18.3 |
| A | 0.733 (20) | 20.0 |

(by about 40%) and thus we always use the same pulse. The results of this give interesting insights into the temporal jitter of the laser, however as they are of secondary consequence to the actual teleportation experiment they are given in App. B.

# 5.1. Weak coherent pulse

## 5.1.1. A single teleportation scan

Shown in Fig. 5.1 is a single run where we have scanned the position of the fiber coupler in spatial mode 1 through the HOM dip. The input source used is the WCP, thus plotted on the Y-axis are the three-fold coincidences that represent detection of either a $|\Psi-\rangle$ or a $|\Psi+\rangle$ state at Alice along with a photon at Bob/Victor (see Chap. 4.4 for details on the specific coincidences required for Bell state detection by Alice). As is always the case, Alice measures in the H/V basis and, because in this run the input state is $|D\rangle$, Bob measures in the D/A basis. Successful teleportation is confirmed by detection of a $|\Psi-\rangle$ state at Alice and a $|D\rangle$ state at Bob or a $|\Psi+\rangle$ state at Alice and an $|A\rangle$ state at Bob (as we do not implement the active feed-forward in these experimental runs). The most obvious feature of Fig. 5.1 is the HOM interference (see Chap. 4.4). When the position of coupler 2 is greater than 9.5 mm or less than 9.1 mm[1] the two photons sent to Alice do not temporally overlap at the FBS and thus we obtain no HOM interference resulting in no Bell state measurement being implemented. However at approximately 9.33 mm we see that maximal HOM interference is obtained. In calculating the teleportation visibility *only* this point is taken into account.

---

[1] The measurement of the coupler position is relative only to some fixed position upon the table, and thus only the relative distances are of importance. Other than that we find the HOM dip somewhere within the movement range of the coupler's electronically controlled micrometer screw.
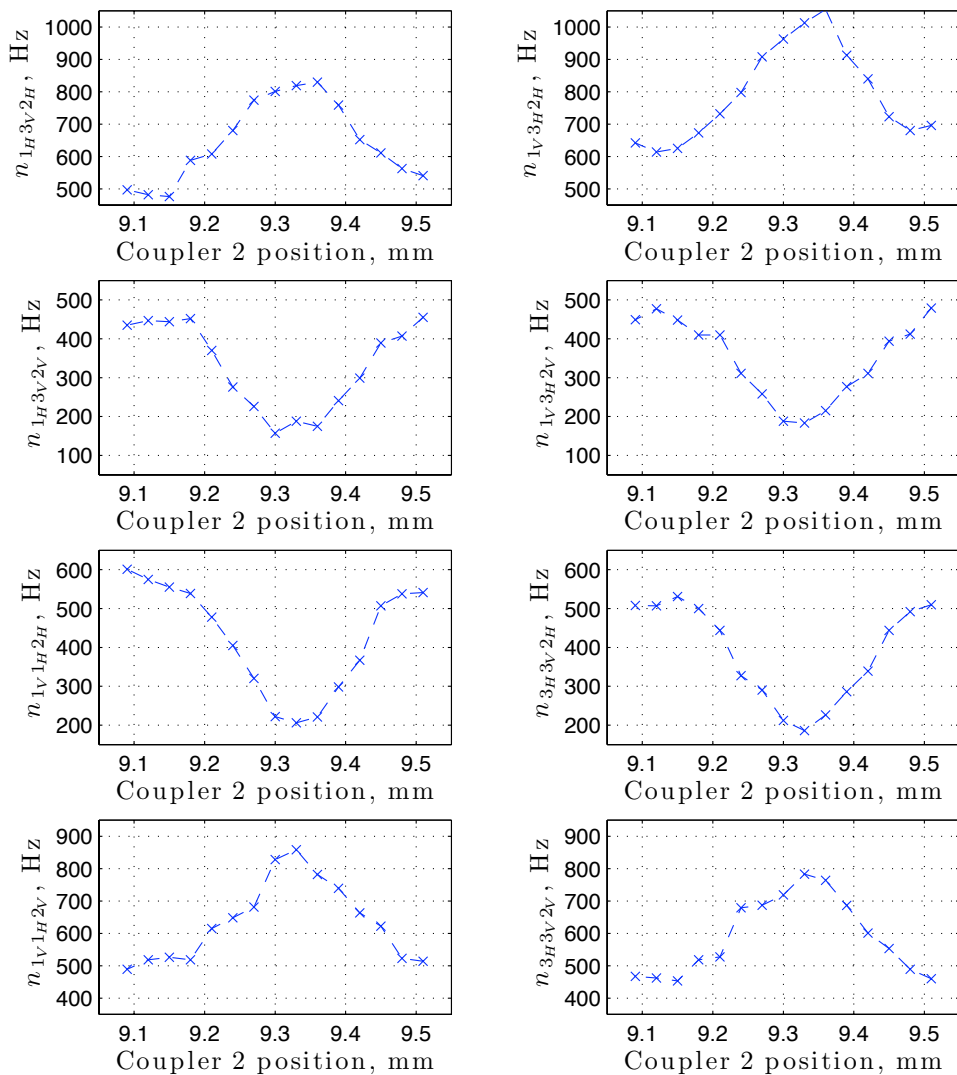
**Figure 5.1.:** Results of a single run of teleportation with the WCP input. The input state is D, all of Alice's detectors are in the H/V basis and Bob's detectors are in the D/A basis. The distinctive HOM peak and dip can be seen, with high fidelity teleportation only occurring at the peak/dip position. The first two plots show successful teleportation where Alice measures a singlet state, the seconds two again are with the measurement of a singlet state at Alice, however with Bob measuring the orthogonal state to the input state. The final four plots are with measurements at Alice of a $|\Psi+\rangle$ state, thus the maximum and minimum values are oppositely correlated with the singlet state results as we do not implement Bob's unitary transformation in this run.

In many of the runs that were completed this point was already known (by scanning the dip first, as in this run) and then we simply measure *only* this point of maximal HOM interference. It is also noted that for the experiment on the Canary Islands we plan to first find the dip position using two-fold coincidences at Alice, then carry out the teleportation by using only this position.

In Fig. 5.1 the first two plots (coincidences $n_{1_H 3_V 2_H}$ and $n_{1_V 3_H 1_H}$ [2]) show successful teleportation where Alice measures a singlet state, the seconds two (coincidences $n_{1_H 3_V 2_V}$ and $n_{1_V 3_H 1_V}$) again are with the measurement of a singlet state at Alice, however with Bob/Victor measuring the orthogonal state to the input state, that is unsuccessful teleportation. The final four plots are with measurements at Alice of a $|\Psi+\rangle$ state, thus successful teleportation is given in the final two plots (coincidences $n_{1_H 1_V 2_V}$ and $n_{3_H 3_V 1_V}$) and unsuccessful teleportation given by plots five and six (coincidences $n_{1_H 1_V 2_H}$ and $n_{3_H 3_V 1_H}$). For this run the WCP was operated with a count rate of 2.07 MHz and the EPR rate, that is $n_{12}$, was 42 kHz. The teleportation visibility where Alice measured a singlet state was 0.693(3) and where Alice measured a $|\Psi+\rangle$ state 0.648(3). The overall teleportation visibility was 0.673(1) which is a 25.3 standard deviation violation of the classical limit (see Ch. 3.2.1).

## 5.1.2. Numerical model

A theoretical model of our setup was made in order to understand the relationship between the parameters in the setup and the teleportation visibility and particularly the various count rates of the EPR source and the Fock and WCP inputs. The model was originally created by Thomas Scheidl and Sven Ramelow, two co-workers in our group, and is meant simply as a guide to understanding the setup and thus has a number of major approximations. These are:

- The probability of $n$ photon pairs is $p^n$, where $p$ is the probability of a single pair.

- The model is first order, that is it ignores any errors given by the detection of 5 or more photons.

- It does not account for the fact that increasing the coincidence window beyond a single pulse of the laser will give a finite probability for the detection of photons from other pulses.

- It ignores any dark counts at Alice.

---

[2] It is noted that with Alice measuring in the H/V basis and Bob/Victor measuring in the D/A basis a coincidence count $n_{1_H 3_V 2_H}$ report coincidence detection of a horizontally polarised photon in spatial mode 1, a vertically polarised photon in spatial mode 3 and a diagonally polarised photon in spatial mode 2.

- There is a single parameter (the system visibility) that corrects for all experimenter errors. These include errors such as non perfect polarisation alignment, poor compensation for walkoff effects or misalignment of the central wavelength of the interference filters.

The core of the model is a set of equations that calculate the probability that in any pulse of the laser we record a 'true' teleportation result, or that we record a four-fold coincidence from some form of error. For the Fock input these take the form:

$$\text{p4FTrue} = \frac{1}{2\,\omega^2}\big(n_{12}\,n_{34}\big) \tag{5.1}$$

$$\text{p4FErrBBO1} = \frac{1}{\omega^3}\left(\frac{1}{6}n_1\,n_{12}\,n_4 + \frac{1}{4}n_1\,n_2\,n_{34}\right) \tag{5.2}$$

$$\text{p4FErrBBO2} = \frac{1}{\omega^3}\left(\frac{1}{6}n_2\,n_3\,n_{34} + \frac{1}{4}n_{12}\,n_3\,n_4\right) \tag{5.3}$$

$$\text{p4FErrNB} = \frac{1}{\omega^3}n_{dc\,2}\left(\frac{1}{8}n_1\,n_{34} + \frac{1}{12\,\omega}n_1^2\,n_4 + \frac{1}{6}n_3\,n_{34}\right), \tag{5.4}$$

where $\omega$ is the repetition rate of the laser (80 MHz) and $n_{dc\,2}$ is the rate of dark counts at Bob (both detectors, in Hz). The four terms are, respectively, the probability of a four-fold coincidence due to the detection of a pair from both sources (what we call 'true' teleportation above), the probability of a four-fold coincidence with an error from the EPR source, with an error from the Fock input and finally from a dark count at Bob respectively. Using these terms we can calculate the teleportation visibility as well as the rate at which we accumulate statistics, which allows calculation of the time required for a certain violation of the classical limit.

The corresponding terms for the setup using the WCP input are as follows:

$$\text{p3FTrue} = \frac{1}{2\,\omega^2}\big(n_{12}\,n_{\text{WCP}}\big) \tag{5.5}$$

$$\text{p3FErrBBO1} = \frac{1}{6\,\omega^2}\big(n_1\,n_{12}\big) \tag{5.6}$$

$$\text{p3FErrCoh} = \frac{1}{8\,\omega^3}\big(n_{\text{WCP}}{}^2\,n_2\big) \tag{5.7}$$

$$\text{p3FErrNB} = \frac{1}{\omega^3}n_{dc\,2}\left(\frac{1}{4}n_1\,n_{\text{WCP}} + \frac{1}{8}n_{\text{WCP}}^2 + \frac{1}{6}n_1^2\right) \tag{5.8}$$

The four terms are as above however all the coincidences are three-fold coincidences, 'true' teleportation is the detection of a pair from the EPR source and a single photon from the WCP input and an error from the Fock input is exchanged for an error from the WCP input.

For the source code actually used to implement the model see App. C. The results gained using this are discussed in the next section.

### 5.1.3. Optimal count rates

Due to the large attenuation induced because of the link between the two Canary Islands it is important to understand the relationship between the count rates and the total time needed to give a certain violation of the classical limit. As stated previously, increasing the count rate will necessarily increase the error rate, thus decreasing the overall teleportation visibility. However, increasing the count rate will also increase the rate at which we can demonstrate teleportation and thus decrease the time taken to show a violation of the classical limit.

Figure 5.2 below shows a series of runs with various EPR and WCP rates and the prediction of the numeric model. The measurements given in this figure were performed on a previous setup that we built in the laboratory. This previous setup was very similar to the current one with the major difference that both down-conversion BBO's used type-II *non*-collinear down-conversion, thus the Fock state source was actually entangled in polarisation, although this entanglement wasn't actually used. Further details about this source can be found in App. D. The measurements were made with no attenuation in the link to Bob.
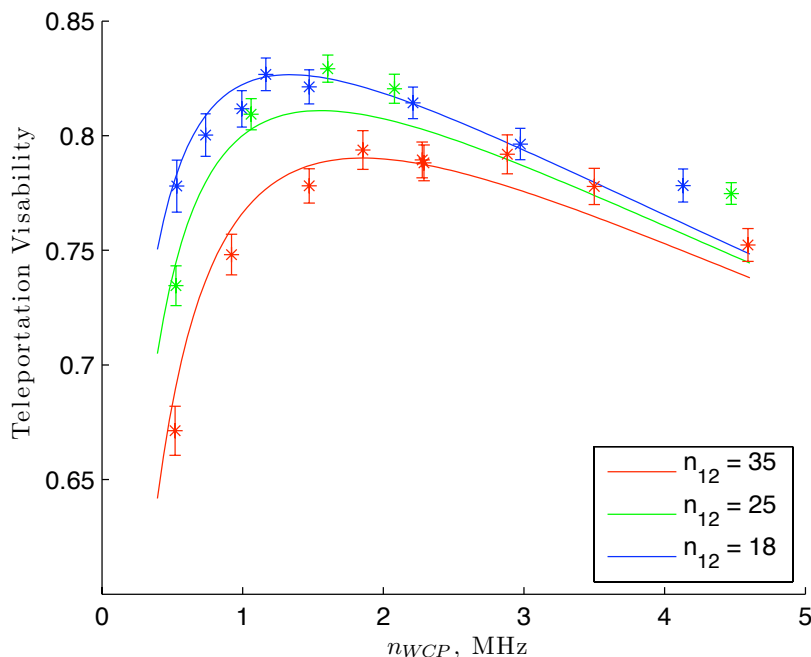


**Figure 5.2.:** Comparison of experiment with the numerical model for the WCP on the previous experimental setup. The measurements were completed in July, 2009. Integration times are between 20 and 180 seconds and $\eta_1 = 0.098$ and $\eta_2 = 0.176$. For the measured values the colour of the point indicates the EPR rate ($n_{12}$) in exactly the same manner as for the theoretical curves.

Firstly the figure shows reasonable agreement between the model and the experimental results lending support to the validity of the model. Also it can be seen that for every EPR rate there is some optimal WPC rate that gives the maximum teleportation visibility. There also exists a WPC rate that gives the minimum time to show a certain violation of the classical limit. This is slightly higher than the rate that gives the maximum teleportation visibility. [3]

In Fig. 5.3 we show the predicted time taken to realise a three standard deviation violation of the classical limit against the EPR rate, $n_{12}$, and with an attenuation of 30 dB in the link to Bob. For every EPR rate the WCP rate is set to minimise the total time taken. Firstly from the plot it is clear that teleportation with 30 dB attenuation is possible within a reasonable time as confirmed by the visibilities given in Table 5.1. Secondly because (as shown in Fig. 5.2) the achieved visibilities are well above the classical limit (1/3) increasing the count rates decreases the overall time required. The four various curves show different possible coupling efficiencies, $\eta_1$ and $\eta_2$. We also see that because the teleportation visibility is so far above the classical limit, even with coupling below that that has been achieved in the laboratory (see Tables D.1 and 5.3 below) we can still achieve reasonable results in a short time.

Figure 5.4 shows a more detailed look at two of the points plotted in Fig. 5.3. Both plots are with an EPR rate of 60 kHz, however the left hand side plot shows the time for a 3 standard deviation violation of the classical limit, and the right hand side plot shows time for a 12 standard deviation violation. These plots clearly show the trade off between optimal visibility or optimal standard deviation violation as a function of the WCP rate. As we may integrate for times longer than even those given for a 12 standard deviation violation we are at liberty to decide upon whether visibility or standard deviation violation is a requirement of the experiment.

---

[3]It is clear in the early era of quantum mechanics, and in some current experiments that seek to disprove certain classes of theories, in particular Bell type experiments, for example [2, 48], showing violation of the classical limit is of importance. However in this work we aim to demonstrate long distance teleportation. Although the nomenclature of the field is such that teleportation is generally called 'quantum state teleportation', classical teleportation is a farcical concept (as we can show that such teleportation would be limited to a fidelity of one half). Although it is a matter of definition, it is my opinion a scheme that could not, even in theory, realise unit fidelity should not be called teleportation and thus there is no arbitrariness if one were to call 'quantum state teleportation' simply teleportation.

In this work we are left in a situation where have a bright enough source that we can (in particular with the WCP) turn down the count rates used, thus increasing the teleportation visibility but reducing the classical violation. It is my personal opinion that in such a situation lower count rates should be used, as the goal of teleportation is the exact copying of a system from one position to another without moving the system between the points, thus how exactly one can copy that system is of central importance to the scheme.
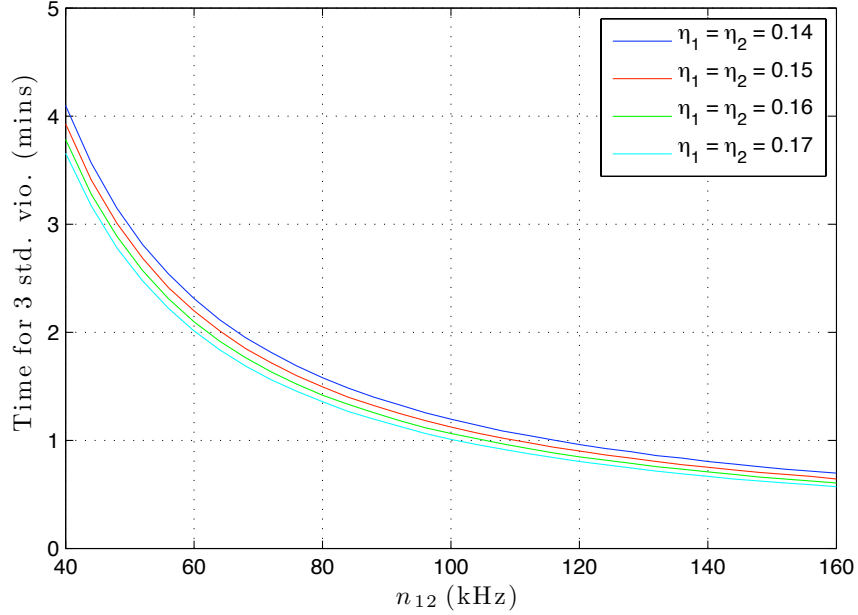
**Figure 5.3.:** Theoretical prediction from the numerical model for the optimal count rate of the EPR source for a three standard deviation violation of the classical limit. The WCP rate always at the optimal rate for the given EPR rate.
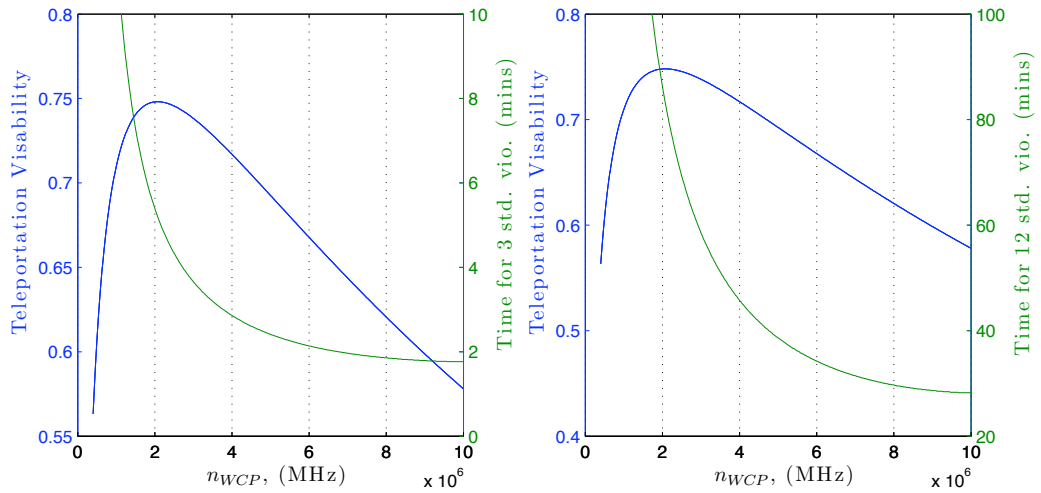


**Figure 5.4.:** Predicted visibility and time needed to violate classical limit with the WCP setup. $n_{12}$ has been set to 60 kHz, $\eta_1$ to 0.160 and $\eta_2$ to 0.139. The left hand plot is for a 3 standard deviation violation of the classical limit and the right hand plot for a 12 standard deviation violation.

## 5.1.4. Parameter range of setup

In Chap. 5.1.3 above we discussed the possible visibilities and times required for a certain violation of the classical limit given the quality of the setup. Here we give an overview of the count rates and coupling efficiencies of the source to make clear what is possible with the setup and what is beyond its limits.

Given in Table 5.3 are the approximate count rates and coupling efficiencies obtainable from the source. The values are taken from work in February 2010. Note that all count rates are measured without attenuation. Also note that the singles counts and coincidence counts are counted independent of polarisation. This data illustrates the quality of the setup with the source being used as a brighter source. It would be possible to increase the coupling slightly by using a smaller pinhole aperture (see Chap. 4.3.2), however this would reduce the count rate of both sources thus dramatically reducing the four-fold count rate. No values are given for the coherent pulse as the count rate was fully tunable, and the coupling is not defined, as the input is not paired with another photon. However the count rate used for the coherent pulse was generally in the range 1.2 to 3 MHz.

**Table 5.3.:** The count rates and coupling efficiencies of source in February 2010. The values are a characterisation of the source before an experimental run and are deemed to be representative of the quality of the source after optimisation. In addition the entanglement visibility of the EPR source was approximately 22:1 in the D/A basis and 27:1 in the H/V basis. This visibility is defined as the ratio of pairs with opposite polarisation to pairs with the same polarisation.

| Variable | Value | Variable | Value |
|:---:|:---|:---:|:---|
| $\eta_1$ | 0.157 | $\eta_3$ | 0.103 |
| $\eta_2$ | 0.124 | $\eta_4$ | 0.184 |
| $n_1$ | 573 kHz | $n_3$ | 608 kHz |
| $n_2$ | 725 kHz | $n_4$ | 1087 kHz |
| $n_{12}$ | 90 kHz | $n_{34}$ | 112 kHz |

The values given in Table 5.3 are representative of the quality of the source when it has been optimised. Of course with additional time spent optimising the source one could achieve higher efficiencies and count rates, however large increases in source quality are not expected without major changes to the actual source setup.[4] With these values we see that the parameter ranges given in Figs. 5.3 and 5.4 are obtainable and indeed are obtained as shown by the measured visibilities.

---

[4]By simply tuning the coupling (and the position of the BBO's etc.) it is possible that one to two percent better coupling could be achieved although it would take a significant period of time to gain such improvements.

## 5.2. Fock input

For the Fock state input the teleportation visibility is inherently higher than with the WCP, although the count rates are much lower. In the WCP scheme we do not know exactly when we have an input photon, thus we must include results any time that we measure either a $|\Psi+\rangle$ or a $|\Psi-\rangle$ state at Alice, however this measurement may have come from an error at the EPR source (through the creation of two pairs for example). As we know exactly when we have an input photon with the Fock input we exclude any cases where this photon is not present thus disregarding some of the aforementioned cases where we would have had an error at Alice. The count rates are lower as creating the Fock state photon through SPDC is both an inefficient process and is limited by errors at high count rates, as discussed in Chap. 4.2. The upper limit on count rates used in this experiment, with an acceptable error rate, was approximately 120 kHz, whereas we commonly used a WCP rate of 2 or even 3 MHz. The result of having higher visibility but lower count rates for the Fock input scheme is that although we have some control over the count rates, the optimal counts rates are basically the highest count rates possible. Although we must still use the pinholes to preserve high quality coupling (greater than approximately 10%), as given in Chap. 4.3.2. Thus the results for the Fock input are almost completely summed



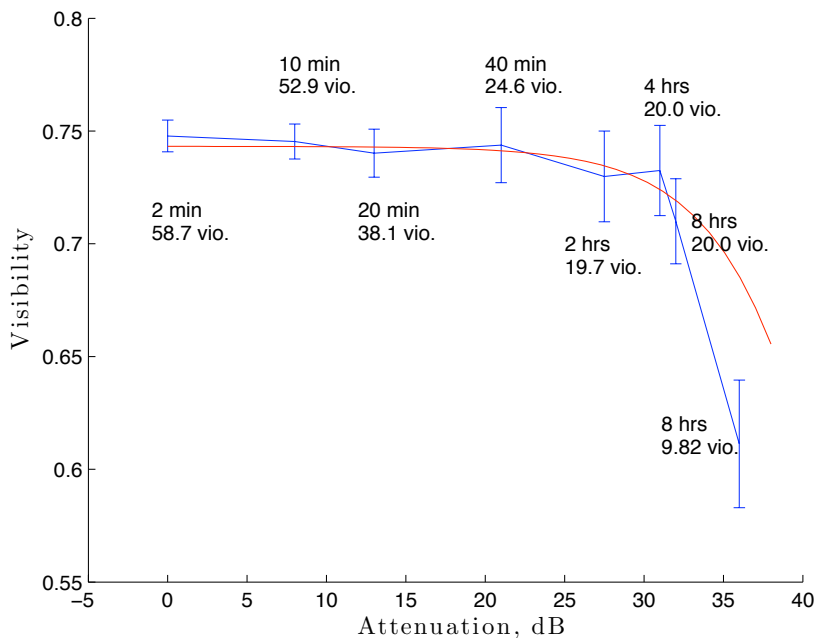**Figure 5.5.:** Teleportation visibility with attenuation with Fock state input. The measurements were completed in April, 2010. Integration times and classical violation in standard deviation given for each point. $n_{12} \simeq 104$, $n_{34} \simeq 111$, $\eta_1 \simeq 0.124$, $\eta_2 \simeq 0.152$, $\eta_3 \simeq 0.102$ and $\eta_4 \simeq 0.173$. The red curve is the prediction of the model given the parameters used.

up in Fig. 5.5. These results are obtained with an EPR rate of 90 kHz and a Fock input rate of 110 kHz. The input state used is $|A\rangle$. The most notable feature of Fig. 5.5 is the strong drop in visibility beginning around and attenuation of 30 dB. This is a result of the signal to noise ratio becoming comparable at this point, as explained in the next chapter, Chap. 5.3. It can also be seen that even at an attenuation as high as 35 dB we are able to obtain both a very confident violation of the classical limit and high teleportation visibility within 8 hrs. Also at very high attenuation we find some deviation between the model and the results, this in part can be accounted for by the degradation of the source over the period of the experimental run, which is not taken into account for by the model. In addition we assume that the dark counts are 'white noise' and if some of these counts are correlated with the laser pulses then this would increase the effective dark counts, accounting for the behaviour seen.

Shown in Fig. 5.6 we see the accumulation of the standard deviation with time for the longer scans. The data here was recorded at 31 dB attenuation, and with count rates almost identical to that given for Fig. 5.5. It can be seen that the classical limit violation with an input state of $|H\rangle$ is much higher than with $|D\rangle$, $|A\rangle$ and $|R\rangle$. This is firstly as the entanglement visibility in the H/V basis is better than in other bases due to the fact that the type-II non-collinear SPDC creates a horizontal and a vertical photon, but only at the crossing point, and with the correct phase between these photons, will this results in orthogonally polarised photons in the other two bases and also because Alice measures in the H/V basis, thus the correlations (which could be described perfectly within the framework of classical mechanics) between the particles alone insure teleportation *without* requiring the HOM interference, this is not the case for the other bases. More importantly Fig. 5.6 shows that even in short times, as little an hour, we could successfully teleport a quantum state in all bases. In addition these measurements are complementary to the 31 dB measurement given above, that is the visibility of the states $|D\rangle$, $|A\rangle$ and $|R\rangle$ are around 0.74, while that of $|H\rangle$ is approximately 0.85.

## 5.3. Measurement

Measurement at Alice was completed using four fiber coupled single photon detectors (actively quenched avalanche photo diodes). The total dark counts over all four detectors was approximately 1400 Hz, ranging from 200 to 500 Hz per detector. However the exact dark counts at Alice are not as important as the actual single count rates arriving at the detectors was in the hundreds of Kilohertz, and even the three-fold ($n_{134}$ for the Fock state input) or two-fold ($n_{13}$ with the WCP input) coincidences were at or above Kilohertz. Thus the signal to noise ratio was very good.

Because of the 30 dB attenuation introduced in the link to Bob the dark counts

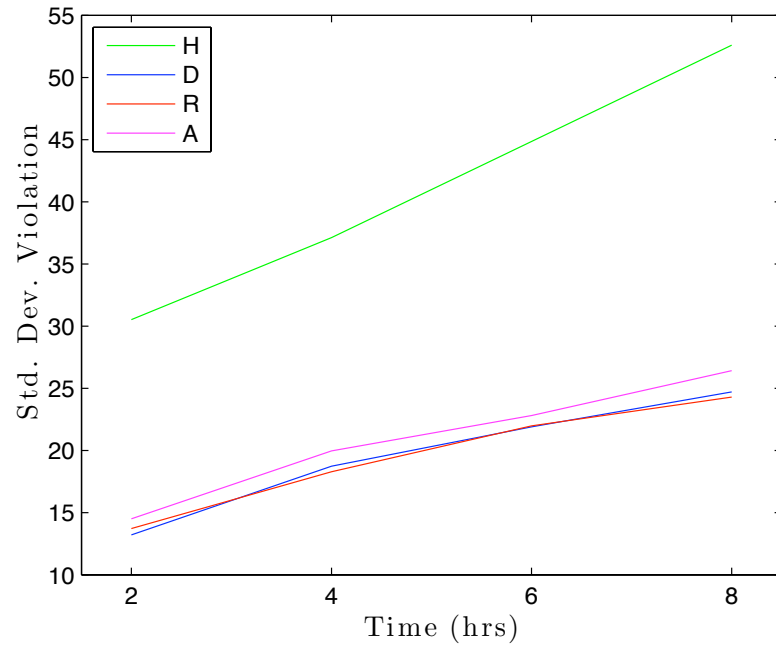**Figure 5.6.:** Accumulation of standard deviation violation of classical limit with Fock state input for input states H, D, R and A. The measurements were completed in April, 2010. The visibilities for states D, R and A are approximately 0.74 and that of H was approximately 085. $n_{12} \simeq 104$, $n_{34} \simeq 111$, $\eta_1 \simeq 0.124$, $\eta_2 \simeq 0.152$, $\eta_3 \simeq 0.102$ and $\eta_4 \simeq 0.173$.

at his/Victor's module are much more important. Figure 5.7 shows the relationship between dark counts at Bob/Victor (the total on both of his detectors) and the teleportation visibility. The curves show the predicted results from the numerical model, and the points given are measured on the old setup, both are for the WCP input. It can be seen that at about the 30 dB attenuation mark the visibility begins to drop off and by approximately 40 dB the visibility is already below the classical bound. This behaviour is also confirmed in Fig. 5.5 in Chap. 5.2.
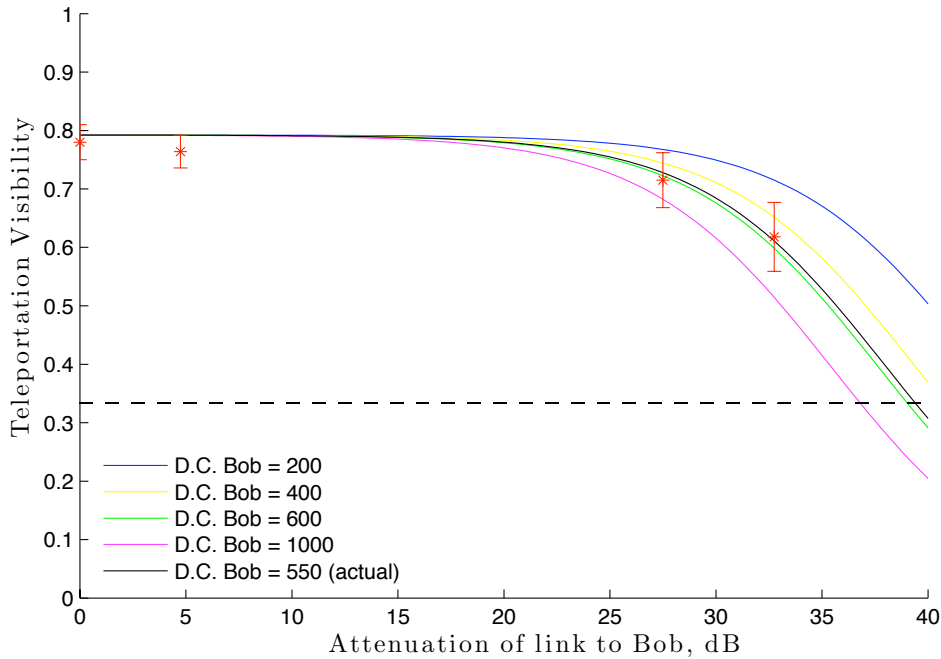


**Figure 5.7.:** Prediction and measurements for the teleportation visibility with attenuation with a WCP input. The measurements, given in red, were measured on the old setup. The measurements were completed in August, 2009 and the experimental parameters were as follows: $n_{12} = 36$ kHz, $n_{\mathrm{WCP}} = 1.41$ MHz, $\eta_1 = 0.104$, $\eta_2 = 0.178$ and the total dark counts at Bob/Victor were 550 Hz. The parameters for the simulation follow these except the dark counts, which are as given.

The finite dark counts at Bob are one of the two major theoretical difficulties[5] caused by completing an experiment between the Canary Islands, the other being

---

[5]In principle the attenuation introduced by the link between the two Islands is only a problem because of the dark counts at Bob, and because of the increased integration time required to demonstrate teleportation. However many other practical problems exist in setting up an experiment between the Canary Island although the details of these problems are outside the scope of this work.

that one must simply integrate for a longer period of time to gather enough statistics to demonstrate successful teleportation. To understand this difficulty we consider the following simple model.

The probability of successful teleportation in any pulse from the laser is

$$p_s = p_{\text{BSM}} \, \eta_2 \ , \tag{5.9}$$

where $p_{\text{BSM}}$ is the probability that in that pulse Alice records a successful measurement of either $|\Psi\pm\rangle$ with a coincidence with $n_4$ where a Fock state input is used, and we note that $\eta_2$ is the coupling to Bob, which includes the attenuation of the link (see Chap. 4.3 for the definition of coupling efficiency). The probability of an error due to the dark counts at Bob is similarly given by,

$$p_n = p_{\text{BSM}} \, n_{dc} \, \tau_{cw} \ , \tag{5.10}$$

where $n_{dc}$ is the dark count rate (in Hz) and $\tau_{cw}$ is the coincidence window used in our logic (in s). The signal to noise ratio is thus

$$\text{SNR} = \frac{p_s}{p_n} = \frac{\eta_2}{n_{dc} \, \tau_{cw}} \ . \tag{5.11}$$

Using approximate values in equation 5.11 we have

$$\text{SNR}_{30 \text{ dB}} \approx \frac{10^{-4}}{10^3 \, 10^{-8}} = 10 \ \text{ and } \ \text{SNR}_{40 \text{ dB}} \approx \frac{10^{-5}}{10^3 \, 10^{-8}} = 1 \ . \tag{5.12}$$

From the definition of visibility we see that in the case of 30 dB attenuation the overall teleportation visibility is reduced by 9%, and at 40 dB the visibility would be 50% lower, in good agreement with the predictions and results given in Fig. 5.7.

As discussed in Chap. 4.3 much effort was put into increasing the coupling $\eta_2$. In Eq. 5.11 we see that with large attenuation the dark counts at Bob and the coincidence window are equally important in maintaining high teleportation fidelity. To reduce the dark counts first of all the detectors are mounted in a light-proof box, to stop stray light from the room (from either the room lights or indirectly from the laser) reaching the detectors. In addition we have control over the bias voltage of Bob's detectors. Low bias voltage will give lower dark counts, but also reduced coupling, $\eta_2$ (as the detector quantum efficiency will be reduced). Increasing the bias voltage will increase both the dark counts and $\eta_2$. Thus we seek to find the bias voltage position that gives the best SNR, or equivalently the best teleportation results.

In Fig. 5.8 we show the measured single count rate of the detectors and the detector dark counts with the bias voltage of the detectors. The expected scaling noted above is clearly seen. In fig. 5.9 we then show a simulation of the time required for a three standard deviation violation of the classical limit with

parameters taken from Fig. 5.8 and in other cases usual experimental values experienced. Due to the 10 V bias voltage offset between the two detectors we set the voltage of APD2 to be 10 V more than APD1. It can be seen that at about 206 V (for APD1) the setup works most efficiently, thus this is the value we used throughout this work.
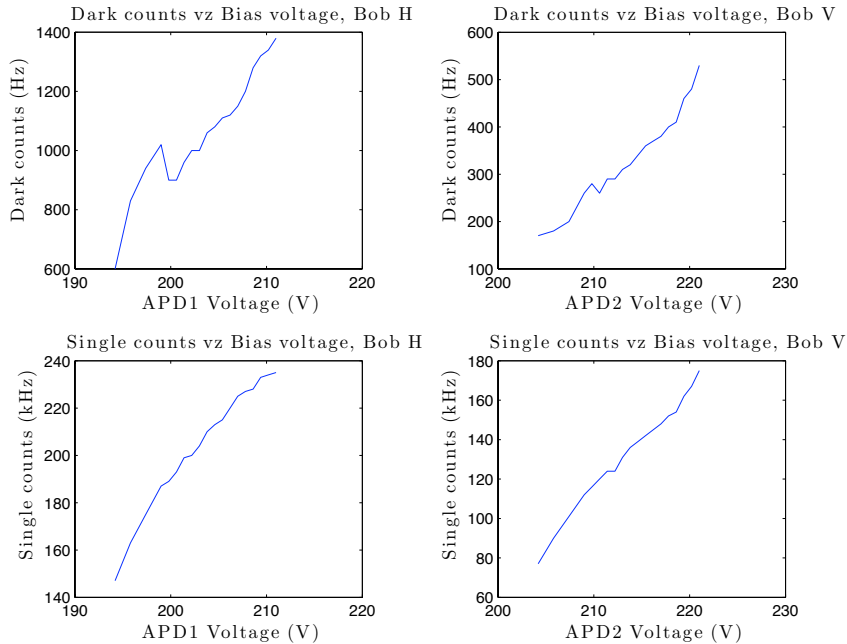


**Figure 5.8.:** Detector count rate and dark count count rate plotted against bias voltage. The first two plots give the dark counts with the bias voltage for APD's 1 and 2 and the final two plots give the single count rates. The absolute count rate is not of central importance, rather the drop in the detector quantum efficiency. Data recorded in March, 2010.

In addition to tuning the dark counts we may also set the coincidence window of the logic. As explained in App. A.4 we may set the number of bins for which the coincidence window is open, which corresponds to a setting the temporal length of the coincidence window. In Fig. 5.10 we show the teleportation visibility with the coincidence window. It can be seen that a coincidence window below 6 ns allows high quality teleportation. We also see in Fig. 5.10 that the teleportation where Alice measures a $|\Psi+\rangle$ state has consistently lower visibility. This can be explained by an imbalance between the count rates recorded at different detectors. If the coupling of detector $D2_H$ is better than that of detector $D2_V$ (as is the case here) then more of the correct counts (with Alice measuring $|\Psi-\rangle$) and more of the errors (with Alice measuring $|\Psi+\rangle$) will be measured on these detectors. Thus, as we have not implemented the active feed-forward in these measurements, additional counts at detector $D2_H$ will result in increased visibility for the $|\Psi-\rangle$ state teleportation and decreased visibility for the $|\Psi+\rangle$ state, exactly as given
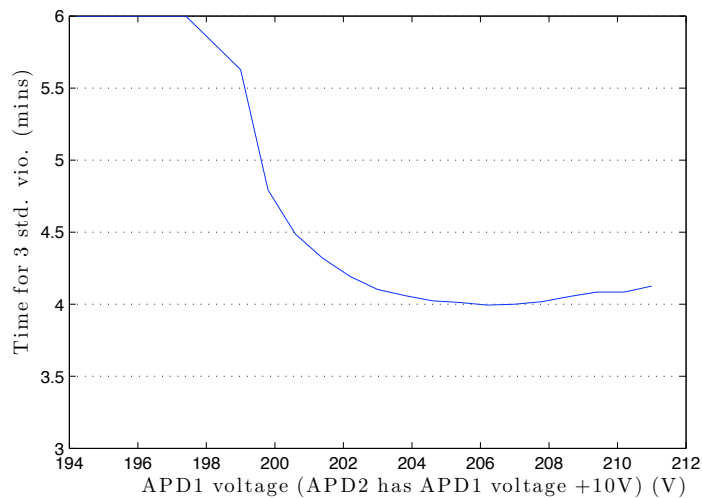
**Figure 5.9.:** Simulation of the time it would take for a three standard deviation classical violation where the dark counts and detector dark and efficiency at Bob are taken from Fig. 5.8. Due to the 10 V bias voltage offset of the two detectors we set the voltage of APD2 to be 10 V more than APD1.

in Fig. 5.10.

The coincidence logic used throughout this work has the limitation that the minimum coincidence window is fundamentally limited by bin size used by the logic. To get around this limitation we also have the possibility to use a time tagging system to find the coincidences. This time tagging system simply gives a tag that records the time of detection of each photon to each photon. We can then electronically adjust the delay of the various detectors to find the correct temporal position of the coincidences between all the detectors. However because of some jitter in the the detection time and within the electronics we must allow some finite sized coincidence window within which we allow single detection events to lead a coincidence event. The main advantage of this technique is that we may adjust the coincidence window with full freedom, although this technique is computationally a little more demanding as it produces a large amount of data.

In Fig. 5.11 we show the measured visibilities and standard deviation violation with the coincidence window. Of particular importance is that in this plot the data is taken with 31 dB attenuation. Similar behaviour to Fig. 5.10, with lower visibilities at larger coincidence windows. However clear differences between the two plots exist, mostly due to the large range of coincidence window used and the different attenuation. As we extend the coincidence window beyond this value the teleportation visibility is strongly reduced. The laser operates at a frequency of 80 MHz, thus the time between laser pulses is approximately 12.5 ns. We see that opening the coincidence window to times that overlap with a second pulse
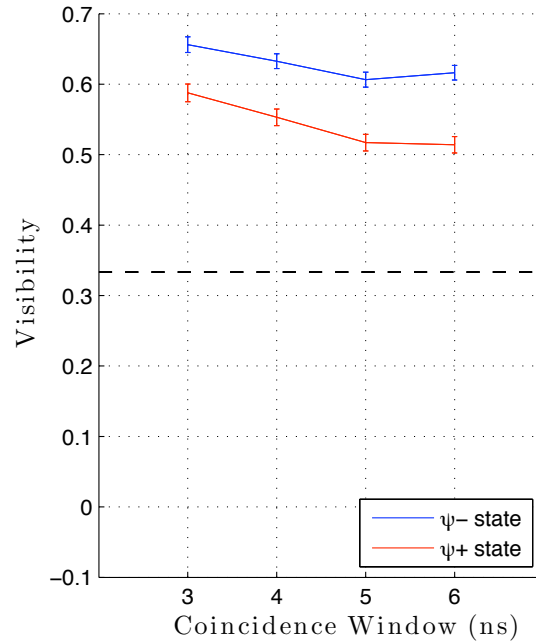
**Figure 5.10.:** Teleportation visibility with coincidence window. The actual coincidence window width is not single value, and can actually be approximately 1.5 ns longer than the values given. See App. A.4 for further details. Data recorded in March, 2010, the attenuation is 0 dB.

causes many errors from coincidences with photons from the pulse before or after the correct pulse. Interestingly in the plot of standard deviation violation we see that with the shortest coincidence window we do not gain the highest violation of the classical limit despite having by far the highest visibility. This is because with such a low coincidence window we cut out a large number of actual teleportation events and thus the error bar on this measurement is somewhat larger than in the measurements with a larger coincidence window.

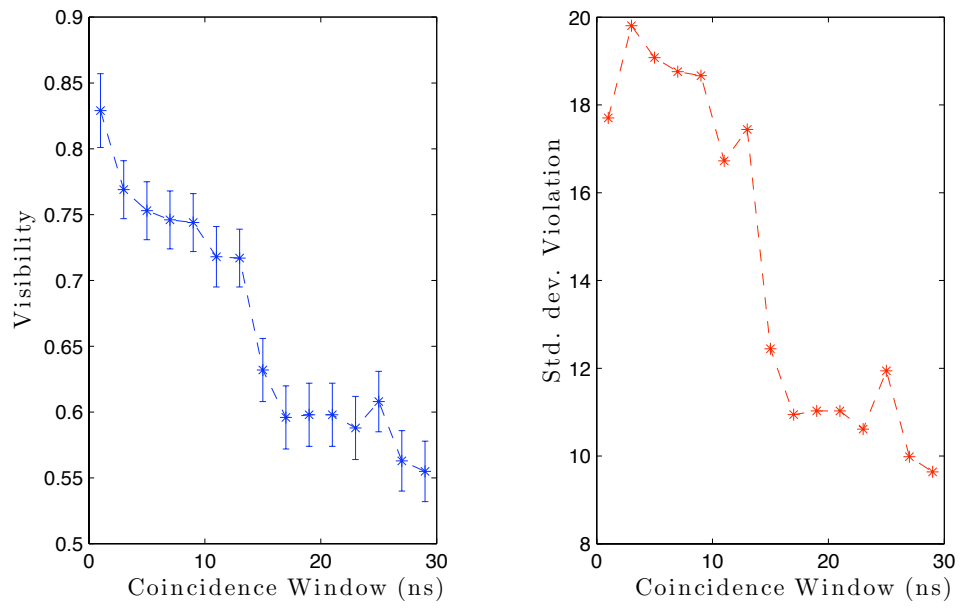**Figure 5.11.:** Teleportation visibility with coincidence window using time tagging with 31 dB attenuation. We see that increasing the coincidence window records more values (indicated by the error and equally the violation of the classical limit) however larger coincidence windows also lead to lower visibilities. Also seen is the drop in visibility due to errors from the neighbouring pulse. Data recorded in March, 2010.

# 6. Conclusion and Outlook

The main goal of this work is to prepare a teleportation setup that is both bright and error free enough to cope with the approximately 30 dB loss that would be encountered in the link between La Palma and Tenerife. With the exception of the active feed-forward component of the teleportation scheme this has been achieved. We show teleportation with average visibility of 0.782(10) with four hours integration time for each basis and with 31 dB attenuation in the link to Bob and a Fock state input photon. This is a roughly 45 standard deviations greater than the classical limit.

In addition we have implemented a WCP input, which is a very bright teleportation setup, and with 31 dB has shown teleportation with a visibility of 0.737(5) in 3 hours, some 80 standard deviations higher than the classical limit. A simple model of the setup has been developed so that the teleportation visibility and count rate can be predicted for given WCP and EPR source count rates. This allows us to quickly tune the setup so as to best demonstrate quantum state teleportation given the link quality experiences in the Canary Islands. Also from the results above we see that, even with times as little as 15 minutes per basis, we can show teleportation that clearly violates the classical limit is achievable with both input sources.

Despite these successes some obvious challenges lie ahead. First we must implement the active feed-forward in a manner that can be used in the Canary Islands. We have already partially implemented this feed-forward in the laboratory, using a Pockels cell triggered by a new in house build coincidence logic. However the optical coding and decoding of the signal so that it may be sent between the two islands has yet to be finalised.

Finally, of course, the actual experiment between the Canary Islands must be carried out. This will require taking the setup apart and then building it back together on La Palma, establishing the optical link between the two Canary Islands and then actually carrying out the runs necessary to demonstrate teleportation.

# Appendices

# A. Experimental techniques

## A.1. Scanning for the HOM dip

A large amount of time was spent finding the point of optimal HOM interference: the 'HOM dip', therefore we will discuss this process in a semi 'how to' manner.

As we already have the photons confined to single mode fibers and filtered with 3 nm interference filters the task here is simply to find the point at which the two photons have exactly zero temporal delay between them. Due to the approximate Gaussian spectral profile of the photos the HOM dip is also approximately Gaussian in shape and has a width of 0.083(2) mm (this value is taken from our experimental results). To obtain the temporal overlap of the photons we use delay stages before all of the inputs to the FBS. For the Fock input this delay is simply realised by moving the position of the coupler with a micrometer screw and where larger temporal delays are required, by changing the length of fiber connecting the FBS and the coupler. Because we have essentially unlimited power for the WCP input we use a free space delay stage with a pair of mirrors controlled by a micrometer screw. This allows us to easily change the temporal delay of this input, although it is unsuitable for the other two sources (due to the losses from the mirrors in coupling back into fiber). For the EPR paired photon we use a combination of micrometer screw and the possibility of different fiber lengths, however in this case the micrometer screw is controlled electronically. See Fig. A.1 for the layout of these components.

Firstly we find the approximate (within less than 0.02 ns) position of temporal overlap with a start stop counter[1]. To do this we use the various input sources (EPR, Fock or WCP) as a 'start' signal and strong laser light directly from the laser as a 'stop' signal[2], this gives the time delay between an arbitrary (but constant) pulse of the laser and the various inputs. Then this time delay is compared with the other time delays of interest. We also only ever align one teleportation scheme at once, that is we either align the EPR and the Fock or the EPR and the WCP, but never all three. To adjust the temporal delay between the various inputs we use additional lengths of optical fiber at first, then for precise alignment the micrometer screws of either the Fock or the WCP are

---

[1] We use a Universal Time Interval Counter, Model No. SR620 made by Stanford Research Systems.

[2] The Coherent Chameleon laser that we use has a TTL output which denoted the time of each pulse and we use this directly with the start stop counter.

used. Finally using the EPR photon's micrometer screw (which is electronically controlled) we scan for the position giving the highest quality HOM interference. This position is easily found by setting both inputs (EPR and Fock or WCP) to the same polarisation and looking for a 'dip' in two-fold coincidence. Because this two photon state is spatially symmetric when the temporal overlap is perfect there should be no coincidence counts however when the two photons are temporarily misaligned they do not interfere and as usual 50% of the time there will be a coincidence.

Regarding the stability of the dip position, it was found that any change in the setup was very likely to change the dip position. Even if the coupling was adjusted this difference was noticed, and the exact dip position had to be scanned again (although generally it would move a fraction of a millimetre if only the coupling was changed). However if the setup was left alone, and only the polarisation aligned, then the dip position was very stable up to time scales of at least a five days. Longer time scales were not investigated enough to comment upon.

## A.2. Diagram of the complete setup

See the following page.

## A.3. Polarisation alignment

Because the final experiment will be completed on the Canary Islands with a tight time schedule we must be able to change from one input type to the other in a short period of time. In addition we must be able to align the polarisation over the 144 km link. We have tried a few methods of polarisation alignment and now use a combination of fiber polarisation controllers (FPC's) and wave plates.

Initially we simply used FPC's, however the polarisation of the photons in spatial modes 1 and 2 (from the EPR source) must be aligned in all three bases, and this proved too time consuming with only FPC's. We tried using the FPC's to align one basis (H/V) and then a BBO (used simply as a birefringent material) to align the other two, however with this method we were only able to obtain a polarisation contrast of approximately 80:1.

The method we now use, again relies upon the FPC's to first align spatial modes 1 and 2 in the H/V basis, then a combination of QWP then HWP then QWP are used to align the other two. The first QWP is aligned at $+45$ deg from horizontal, and the final QWP at $-45$ deg from horizontal. Then we can align the D/A basis by rotation the HWP the lies between the two QWP's without effecting the H/V basis.

For the Fock state and WCP inputs we will always use a definite polarisation state as input, thus we simply align the basis in which the input state gives
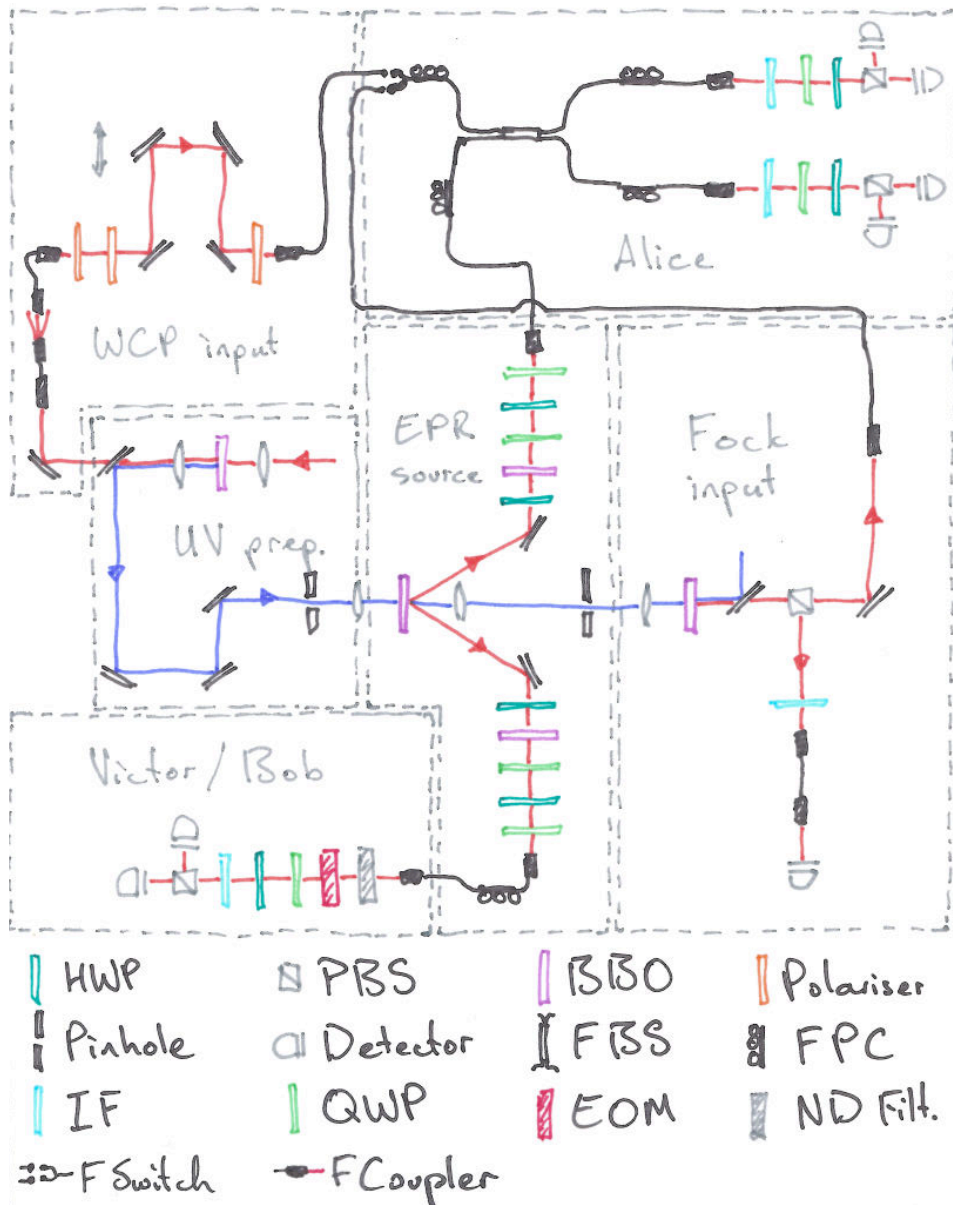
**Figure A.1.:** Setup built in laboratory for long distance teleportation. UV light pumps successively two BBO's, producing two entangled photon pairs. The first pair is used as the entanglement resource and the second as a possible input qubit realised as the spin state of a photon in a Fock state. Additionally strongly attenuated laser light is used as an alternate input source as the polarisation state of light in a coherent state. Alice performs her Bell state measurement with a BS and four detectors. Bob/Victor verify the teleportation. Legend: HWP - half-wave plate, PBS - polarising beamsplitter, BBO - beta-barium borate, FBS - fiber beamsplitter, FPC - fiber polarisation control, IF - interference filter, QWP - quarter-wave plate, EOM - electro-optic modulator ND Filt. - neutral density filter, F Switch - fiber switch, F Coupler - fiber coupler.

maximum contrast using the FPC's, for example if we want to teleport a D state using the Fock input then we simply align the D/A basis of the Fock state. Using this method we are able to achieve polarisation contrast in all relevant bases with greater than 100:1 visibility, and in all cases the visibility is restricted not by the polarisation alignment apparatus, but rather the quality of PBS and detector setup and the dark counts.

## A.4. Electronics

Thus far we have just talked about detectors and detection. However the data from each detector must be read out somehow, and the coincidences between various detection events calculated. To achieve this we use an in-house built coincidence logic box and LabView as the software to read out this data.

The coincidence logic works as follows: The device bins time into 1.56 ns bins. Within the device there will exist signals from the detectors with a corresponding 'internal' signal created by the device and internal signals for each coincidence asked for (up to a maximum allowed amount). Upon receiving a signal from a detector the coincidence logic will trigger the internal signal corresponding to that detector for a length equal to the internal width. The internal width is a parameter set by the user which essentially controls the coincidence window length. The logic then looks for any coincidences as defined by the user. For example, as in Fig. A.2, if we ask for the coincidence counts between detectors D1 and D2 (that is between counts $n_1$ and $n_1$) then the logic will start a new internal signal for coincidences between D1 and D1, along with the two internal signals it starts for detectors one and two. A coincidence is measured simply by looking for overlap of the correct set of signals. Figure A.2 shows a successful coincidence count between detectors D1 and D2. The count rate is simply the number of rising edges for a given internal signal. We then read out these count rates using LabView. For almost all of the work presented here we use an internal width of 3 bins. This implies a coincidence window of somewhere between 3.12 ns and 4.68 ns, as the exact length of the coincidence window depends upon when exactly the detector clicks arrive relative to the time binning of the logic.

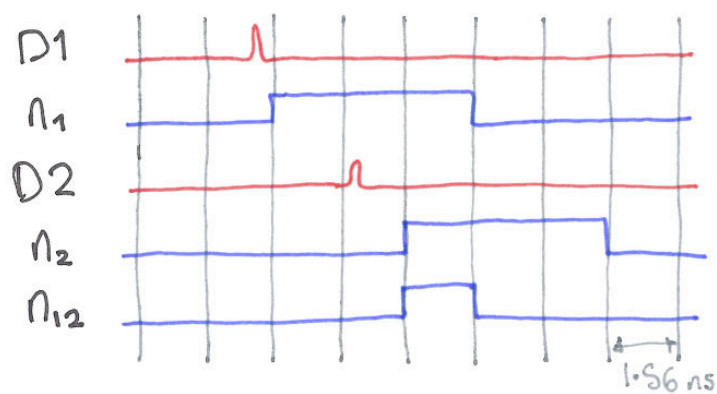**Figure A.2.:** Diagram showing coincidence logic with internal width of 3 bins. Time is first binned into 1.56 ns bins. A signal from a detector (D1 or D2 in this case) will trigger an internal signal of length equal to the internal width. Coincidence, $n_{12}$, looks for overlap of the internal signals ($n_1$ or $n_1$ here). The counts are simply the number of rising edges for a given internal signal.

# B. Switching to second pulse

As stated in the main text we tested creating the inputs from two different laser pulses. We delayed the WCP input by 25 ns so that the EPR source photon pair was generated in a pulse of the laser *two pulses after* the pulse from which the WCP input came. As stated this lead to a reduced teleportation visibility (by about 40%) and thus for all of the results given above the input source and entanglement recourse photons come from the same laser pulse.

Approximately 5.09 m of single mode fiber was added between the the WCP delay stage and the FBS delaying the WCP input photon by approximately 25 ns, which is equal to two times the period of the laser. Additionally the length of the delay stage was adjusted to find the positions of temporal overlap between the EPR photon sent to Alice and the WCP photon required for her Bell state measurement. We then made a number of teleportation scans exactly as we had previously to see how this effected the results. It is noted that all this work was completed on the old source (see App. D).

Figure B.1 below shows the results of a scan of the HOM dip using different pulses and the same pulse. The two scans were measured with very similar parameters, namely coupling and count rates. The four plots are the coincidence counts $n_{1H\,3V\,2H}$, $n_{1V\,3H\,2H}$, $n_{1H\,3V\,2V}$ and $n_{1V\,3H\,2V}$ in kHz, that is the full results for detection of a $|\Psi-\rangle$ at Alice. Two features of these plots are clear. Firstly, as already stated, a disparity in the teleportation visibilities and secondly a disparity in the width of the HOM dip. The teleportation visibility for the run utilising different pulses (green) is 0.48(4), if the visibility of this run predicted by the numeric model for parameters used is 0.78. The visibility for the run with the same pulse is 0.78(2). The width of the HOM dip (given by the first standard deviation of the fitted curve (shown in red/purple)) for this run is 0.11 mm

A number of other runs have been made with both setups and from these the error in dip width over different runs is assumed to be around 0.01. Also two runs at lower count rates were made with this 'next pulse' setup in an attempt to increase the teleportation visibility (each time optimising the coherent pulse rate for maximum teleportation visibility). In each case the results were less than those given above, both being $0.46 \pm 0.04$.

We assume that the additional error is caused by temporal jitter between different pulses of the laser. Thus we may model the data, $\text{Data}(x)$, as a convolution between the laser's temporal jitter, $g(t)$ and the original HOM function (an inverted Gaussian) $\text{HOM}(x, x_0)$. Where $x$ is the spatial parameter over which we scan and $x_0$ is the central position of the HOM dip (which is set by the delay
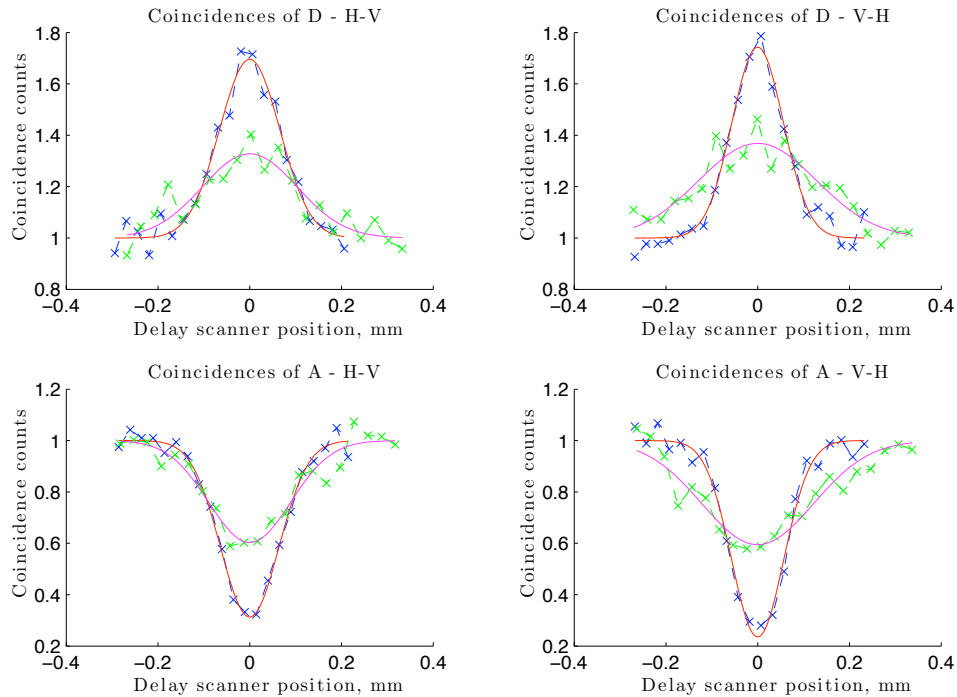
**Figure B.1.:** HOM scan with different pulses.

stages to the FBS and the temporal jitter of the laser. Thus we have

$$\text{Data}(x) = \int_{-\infty}^{\infty} g(x_0)\,\text{HOM}(x, x_0)\,dx_0 \; . \tag{B.1}$$

From this and with the assumption of a Gaussian temporal jitter we may find the measured visibility as a function of the HOM and the laser jitters temporal/spatial width, $\sigma_{HOM}$ and $\sigma_L$ respectively. We also scale this result by the measured HOM visibility, to allow for any systematic errors. This measured visibility $V_M$ is given by

$$V_M = \frac{V_{HOM}}{\sqrt{1 + (\sigma_L/\sigma_{HOM})^2}} \; . \tag{B.2}$$

As we have assumed Gaussian temporal jitter and the HOM interference takes a Gaussian shape the relationship of the three widths, measured, laser and HOM, is simply given as

$$\sigma_M{}^2 = \sigma_L{}^2 + \sigma_{HOM}{}^2 \; . \tag{B.3}$$

Using Eq. B.3 we can calculate that the temporal jitter of the laser is approximately 150 fs, which is of the same order as the pulse duration of the laser. It

is interesting that this method, although containing a number of assumptions, is a form of quantum metrology, where two photon interference is used to measure a laser's temporal jitter. However the precision of the technique, relying heavily upon the precise measurement of different HOM dip profiles, suffers from a number of difficulties not least the controlled scanning of the dip and the precise control of the spectral profile of the light.

After these investigations the setup was returned to its original form and upon doing so we regained the high visibilities previously achieved. Due to the difficulty in improving the temporal jitter of the laser we only use teleportation where all photons come from the same pulse of the laser.

# C. Numerical model of teleportation setup

Given below is the MatLab script used to simulate teleportation using a Fock state input. The first section simply defined all of the values to be used as inputs. All of these values, apart from two, must be single values (integers or floats), and two of the input can be vectors, although not matrices. The main function that calculates the teleportation visibility is then called. This function is also given below. Finally the point with the maximum visibility and the point with the shortest time required to reach the required standard deviation violation (given in the variable nStdVio) of the classical limit are found.

```matlab
1 % Plot 4-Fold Teleportation Visability (Fock input).
2 % File to calculate the teleportation visability and the time to teleport with
      nStdVio of the classical limit.
3
4 clear all
5
6 % ======================= INPUT VALUES ==================== %
7 % ----------------------- MISC. -------------------------- %
8 rR        = 80e6;          % laser repetition rate (Hz)
9 cW        = 3e-9;          % coincidence window (s)
10 attDB    = 31;            % attenuation of link (dB)
11 att      = 1./10.^(attDB./10); %actual atten (I multiply by this number)
12 rN2      = 500;
13 sysVis   = 0.96;          % one minus the percent of max photons that flip
14 nStdVio  = 3;             % wanted in the experiment
15 % ----------------------- COUPLING ---------------------- %
16 eta1 = 0.14;
17 eta2 = 0.15; % LOCAL.
18 eta3 = 0.104;
19 eta4 = 0.174;
20 % ----------------------- 2 FOLDS ---------------------- %
21 r2F1v = linspace(30e3,110e3,60);   % LOCAL.
22 r2F2v = linspace(30e3,110e3,60);   % LOCAL.
23
24 % The first entry below is noted as 'X' and the scond 'Y'
25 [r2F1,r2F2] = meshgrid(r2F1v,r2F2v);
26
27 var1Vect = r2F1v;
28 var2Vect = r2F2v;
29 % ======================================== %
30
31 runTimes = linspace(2,4,2000)*3600;
32 [r4FT,r4FBBO,r4FN,visPer,vis,time] = fourFoldCalc(runTimes,rR,cW,att,rN2,sysVis,
      nStdVio,eta1,eta2,eta3,eta4,r2F1,r2F2);
33
34 rMax    = (r4FT + r4FBBO + r4FN)*sysVis;
35 rMin    = r4FBBO + r4FN + rMax./sysVis - rMax;
```

```
36
37 % PosVis1&2
38 [maxVect,maxPosVect] = max(vis);
39 [maxVal,maxPos]      = max(maxVect);
40 posVis1 = maxPos;
41 posVis2 = maxPosVect(maxPos);
42
43 % PosTime1&2
44 [minVect,minPosVect] = min(time);
45 [minVal,minPos]      = min(minVect);
46 posTime1 = minPos;
47 posTime2 = minPosVect(minPos);
```

The function file containing the main body of the calculation from line 32 of the code above is as follows.

```
 1 function [r4FT,r4FBBO,r4FN,visPer,vis,time] = fourFoldCalc(runTimes,rR,cW,att,
       rN2,sysVis,nStdVio,eta1,eta2,eta3,eta4,r2F1,r2F2)
 2 % function [r4FT,r4FBBO,r4FN,vis,time] =
 3 %    fourFoldCalc2D(runTimes,rR,cW,att,rN2,sysVis,nStdVio,eta1,eta2,eta3,eta4,
       r2F1,r2F2)
 4 %
 5 % Function to calculate the various data from our analytic model. Also note
 6 % that it now assumes that you can recover two of the bell states.
 7
 8
 9 % —————————————— MISC. —————————————— %
10 pN2      = rN2.*cW;
11 rT       = 1./rR;
12 % —————————————— SINGLES —————————————— %
13 rS1  = r2F1./eta2;
14 rS2  = r2F1./eta1.*att;
15 rS3  = r2F2./eta4;
16 rS4  = r2F2./eta3;
17 pS1  = rS1.*rT;
18 pS2  = rS2.*rT;
19 pS3  = rS3.*rT;
20 pS4  = rS4.*rT;
21 % —————————————— 2 FOLDS —————————————— %
22 p2F1 = r2F1.*att.*rT;
23 p2F2 = r2F2.*rT;
24 % —————————————— 4 FOLDS —————————————— %
25 p4FTrue    = p2F1.*p2F2.*(1/4)*2;
26 p4FErrBBO1 = p2F1.*pS1.*pS4.*(1/12)*2 ...
27                + pS1.*pS2.*p2F2.*(1/8)*2;
28 p4FErrBBO2 = pS2.*p2F2.*pS3.*(1/12)*2 ...
29                + p2F1.*pS3.*pS4.*(1/8)*2;
30 p4FErrNB   = pN2.*(p2F2.*pS1.*(1/8) ...
31                + pS1.^2.*pS4.*(1/12) ...
32                + p2F2.*pS3.*(1/12))*2;
33 r4FTrue    = p4FTrue.*rR;
34 r4FErrBBO1 = p4FErrBBO1.*rR;
35 r4FErrBBO2 = p4FErrBBO2.*rR;
36 r4FErrNB   = p4FErrNB.*rR;   % Note that the above values are 'perfect'.
37 % ═══════════════ VISABILITY ═══════════════ %
38 maxVal     = p4FTrue + p4FErrBBO1 + p4FErrBBO2 + p4FErrNB;
39 minVal     = p4FErrBBO1 + p4FErrBBO2 + p4FErrNB;
40 [visPerfect,err,vio] = teleVisMat(minVal,maxVal);
41 [visReal,err,vio]    = teleVisMat(minVal + maxVal − maxVal*sysVis,maxVal*sysVis)
       ;
42 % ═══════════════ ERROR and TIME ═══════════════ %
```

```
43 % Calculate a Matrix of errors for different run times.
44 % runTimes = linspace (2,10,1000)./att(end); % sec as all else in Hz
45 % Used to use this (above) but now have it as an imput to the calculation.
46 rMaxVal   = (r4FTrue + r4FErrBBO1 + r4FErrBBO2 + r4FErrNB)*sysVis;
47 rMinVal   = r4FErrBBO1 + r4FErrBBO2 + r4FErrNB + rMaxVal./sysVis - rMaxVal;
48 maxArr    = zeros(size(rMaxVal,1),size(rMaxVal,2),length(runTimes));
49 minArr    = maxArr;
50 for n = 1:length(runTimes)
51     maxArr(:,:,n) = runTimes(n)*rMaxVal;
52     minArr(:,:,n) = runTimes(n)*rMinVal;
53 end
54 [visArr,errArr,vioArr] = teleVisMat(minArr,maxArr);
55 % Matrix of sizes of std. dev. required for wanted violation.
56 nStdVioArr = ones(size(visArr))*nStdVio;
57 % Now for each mat position calculate the time at which we have the
58 % required number of standard deviation violation.
59 vioTimes = zeros(size(rMaxVal));
60 for n = 1:size(rMaxVal,1)
61     for m = 1:size(rMaxVal,2)
62         [minVal,minPos] = min((vioArr(n,m,:) - nStdVioArr(n,m,:)).^2);
63         vioTimes(n,m) = runTimes(minPos);
64     end
65 end
66 vioTimes = vioTimes./3600;
67
68 % Output:
69 r4FT       = r4FTrue;
70 r4FBBO     = r4FErrBBO1 + r4FErrBBO2;
71 r4FN       = r4FErrNB;
72 visPer     = visPerfect;
73 vis        = visReal;
74 time       = vioTimes;
```

The MatLab script for the WCP input is given below. It follows the same format as that of the Fock input however only one input value may be given as a vector in this case and the main calculation is included directly in the script as opposed to being a separate function.

```
 1 % Plot 3-Fold Teleportation Visability.
 2 % File to calculate the teleportation visability in the H/V and P/M basis.
 3
 4 clear all
 5
 6 % ════════════════ INPUT VALUES ════════════════ %
 7 % NOTE THESE MUST IN TOTAL BE A 1*N VECTOR.
 8
 9 % ──────────────── MISC. ──────────────── %
10 repRate     = 80e6;    % Hz
11 coWind      = 3e-9;   % sec
12 attenDB     = 30; % dB
13 atten       = 1./10.^(attenDB./10); %actual atten (I multiply by this number)
14 rNB         = 550;     % on both detectors at bob.
15 systemVis   = 0.938;
16 numStdVio   = 3;        % wanted in the experiment
17
18 % ──────────────── COUPLING ──────────────── %
19 eta1 = 0.139;
20 etaB = 0.160;
21
22 % ──────────────── SINGLES ──────────────── %
```

```
23  rSC = linspace(0.4e6,10.0e6,500);
24
25  % ———————————— 2 FOLDS ———————————— %
26  r2F1 = 60e3;   % LOCAL.
27
28
29
30  % ═══════════════ CALCULATED VALUES ═══════════════ %
31
32  % ———————————— MISC. ———————————— %
33  pNB     = rNB.*coWind;
34  repTime = 1./repRate;
35
36  % ———————————— SINGLES ———————————— %
37  rS1   = r2F1./etaB;
38  rSB   = r2F1./eta1.*atten;
39
40  pSC   = rSC.*repTime;
41  pS1   = rS1.*repTime;
42  pSB   = rSB.*repTime;
43
44  % ———————————— 2 FOLDS ———————————— %
45  p2F1 = r2F1.*atten.*repTime;
46
47  % ———————————— 3 FOLDS ———————————— %
48  p3FTrue    = p2F1.*pSC.*(1/4)*2;
49  p3FErrCoh  = pSC.^2.*pSB.*(1/16)*2;
50  p3FErrBBO1 = p2F1.*pS1.*ones(size(pSC)).*(1/12)*2;
51  p3FErrNB   = pNB.*(pS1.*pSC.*(1/8)  ...
52                   + pSC.^2.*(1/16)  ...
53                   + pS1.^2.*(1/12))*2;
54
55  r3FTrue = p3FTrue.*repRate;
56  r3FErrCoh = p3FErrCoh.*repRate;
57  r3FErrBBO1 = p3FErrBBO1.*repRate;
58  r3FErrNB = p3FErrNB.*repRate;
59
60  % ═══════════════ VISABILITY ═══════════════ %
61  maxVal     = p3FTrue + p3FErrCoh + p3FErrBBO1 + p3FErrNB;
62  minVal     = p3FErrCoh + p3FErrBBO1 + p3FErrNB;
63  visPerfect = (maxVal - minVal)./(maxVal + minVal);
64  visReal    = visPerfect.*systemVis;
65  [maxVis,posVis] = max(visReal);
66
67  % ═══════════════ ERROR and TIME ═══════════════ %
68  % Calculate a Matrix of errors for different run times.
69  if attenDB > 10
70      runTimes = linspace(1,10,1000)*60; % sec as all else in Hz
71  else
72      runTimes = linspace(0.5,40,1000); % sec as all else in Hz
73  end
74  rMaxVal  = r3FTrue + r3FErrCoh + r3FErrBBO1 + r3FErrNB;
75  rMinVal  = r3FErrCoh + r3FErrBBO1 + r3FErrNB;
76  maxMat   = runTimes'*rMaxVal;
77  minMat   = runTimes'*rMinVal;
78  % Matrix of the error of each coh rate and for each length of run.
79  errorVis = sqrt(((maxMat - minMat)./(maxMat + minMat).^2  ...
80      + 1./(maxMat + minMat)).^2.*maxMat  ...
81      + ((maxMat - minMat)./(maxMat + minMat).^2  ...
82      - 1./(maxMat + minMat)).^2.*minMat);
83  % Matrix of the visibilities above clas. limit for rate and time as above.
84  clasVio = ones(length(runTimes),1)*(visReal - (1.0/3)*ones(size(rMaxVal)));
85  % Matrix of sizes of std. dev. required for wanted violation.
86  wantVio = clasVio./numStdVio;
```

```
87  % Now find the time it takes for the X std. vio for each input vector (of rates)
       .
88  % minPosVect is the position in the TIME vector of the minimum time
89  % required for the specified std. dev. vio. for each rate vect (thus it's a
90  % 1*N vector, as is the input).
91  [minValVect,minPosVect] = min((errorVis − wantVio).^2);
92  vioTimes = runTimes'*ones(1,length(rMaxVal));
93  vioTimes = vioTimes(minPosVect);
94  vioTimes = vioTimes/3600;
95  % Now this is the minimum time for X std. vio.
96  [valStd,posStd] = min(vioTimes);
```

# D. Previous teleportation setup

Previous to setup described in the main text (we will call this the 'main setup' here) another teleportation setup was used to initially investigate the possibility of long distance quantum state teleportation. This setup was used until December, 2009 at which point we began to build the main setup. The setup is shown in Fig. D.1. It is almost identical to the main setup, however both the EPR source and the Fock input were created using Type-II non-collinear SPDC. This does not allow the advantages of the collinear source given in Chap. 4.2 (better coupling efficiency and no need for a polariser) although still functions well as a Fock state source as the required temporal entanglement is still present.

**Table D.1.:** The count rates and coupling efficiencies of old source. The values are a characterisation of the source before an experimental run in September 2009 and are deemed to be representative of the quality of the source

| Variable | Value | Variable | Value |
|----------|-------|----------|-------|
| $\eta_1$ | 0.11 | $\eta_3$ | 0.12 |
| $\eta_2$ | 0.18 | $\eta_4$ | 0.18 |
| $n_1$ | 220 kHz | $n_3$ | 100 kHz |
| $n_2$ | 330 kHz | $n_4$ | 150 kHz |
| $n_{12}$ | 40 kHz | $n_{34}$ | 18 kHz |

Given in Table D.1 are the approximate count rates and coupling efficiencies obtained with the source. Table D.1 represents the averages from work in the lab in September 2009. Note that all count rates are measured without attenuation. The following singles counts and coincidence counts are counted independent of polarisation. It can be seen that the count rates are much less than those used in with the main source, although the coupling is slightly better. This improvement in coupling is mainly due to the pinholes before the down-conversion BBO's giving a greater gain in coupling. Also seen in Fig. D.1 we use two BBO's before the first BBO crystal. Using two BBO's in this manner allowed for this larger gain in coupling efficiency, although it's not fully clear why this was, as using two BBO's at the same distances from the lens that focused onto the BBO's did not induce the same increase in coupling efficiency, and indeed using a second pinhole further from the aforementioned lens did not give any increase at all in coupling efficiency. The addition of the second pinhole in this old setup however increased $\eta_2$ from approximately 0.16 to 0.18, which is a significant increase.
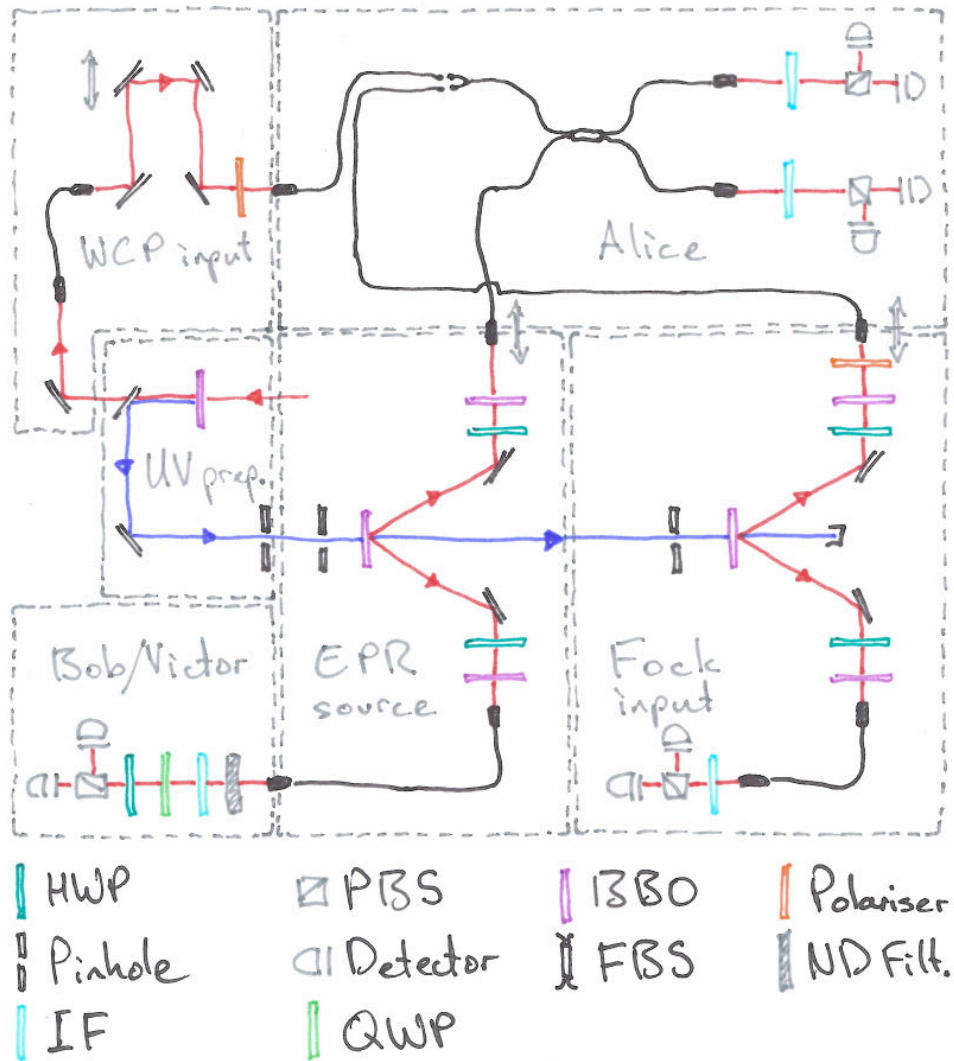
**Figure D.1.:** Previous teleportation setup. UV light pumps successively two BBO's, producing two entangled photon pairs. The first pair is used as the entanglement resource and the second as a possible input qubit realised as the spin state of a photon in a Fock state. Additionally strongly attenuated laser light is used as an alternate input source as the polarisation state of light in a coherent state. Alice performs her Bell state measurement with a BS and four detectors. Bob/Victor verify the teleportation.

# Bibliography

[1] C.O. Alley and Y.H. Shih. New type of einstein-podolsky-rosen experiment using pairs of light quanta produced by optical parametric down conversion. In *Proc. 2nd International Symposium on Foun- dations of Quantum Mechanics in the Light of New Technology*, page 47, 1986.

[2] A. Aspect, P. Grangier, and G. Roger. Experimental tests of realistic local theories via Bell's theorem. *Physical Review Letters*, 47(7):460–463, 1981.

[3] M.D. Barrett, J. Chiaverini, T. Schaetz, J. Britton, W.M. Itano, JD Jost, E. Knill, C. Langer, D. Leibfried, R. Ozeri, et al. Deterministic quantum teleportation of atomic qubits. *Nature*, 429(6993):737–739, 2004.

[4] J.S. Bell et al. On the Einstein-Podolsky-Rosen paradox. *Physics*, 1(3):195–200, 1964.

[5] C.H. Bennett, G. Brassard, C. Crepeau, R. Jozsa, A. Peres, and W.K. Wootters. Teleporting an unknown quantum state via dual classical and Einstein-Podolsky-Rosen channels. *Physical Review Letters*, 70(13):1895–1899, 1993.

[6] D. Boschi, S. Branca, F. De Martini, L. Hardy, and S. Popescu. Experimental realization of teleporting an unknown pure quantum state via dual classical and Einstein-Podolsky-Rosen channels. *Physical Review Letters*, 80(6):1121–1125, 1998.

[7] D. Bouwmeester, J.W. Pan, M. Daniell, H. Weinfurter, M. Zukowski, and A. Zeilinger. Reply: A posteriori teleportation. *Nature*, 394(6696):841, 1998.

[8] D. Bouwmeester, J.W. Pan, K. Mattle, M. Eibl, H. Weinfurter, and A. Zeilinger. Experimental quantum teleportation. *Nature*, 390(6660):575–579, 1997.

[9] S.L. Braunstein and H.J. Kimble. A posteriori teleportation. *Nature*, 394(6696):840, 1998.

[10] S.L. Braunstein and H.J. Kimble. Teleportation of continuous quantum variables. *Physical Review Letters*, 80(4):869–872, 1998.

[11] D.C. Burnham and D.L. Weinberg. Observation of simultaneity in parametric production of optical photon pairs. *Physical Review Letters*, 25(2):84–87, 1970.

[12] J.F. Clauser, M.A. Horne, A. Shimony, and R.A. Holt. Proposed experiment to test local hidden-variable theories. *Physical Review Letters*, 23(15):880–884, 1969.

[13] P.A.M. Dirac. *The Principles of Quantum Mechanics*. Oxford University Press, 4th edition, 1958.

[14] D.P. DiVincenzo. The physical implementation of quantum computation. *Fortschritte der Physik*, 48(9-11):771–783, 2000.

[15] A. Einstein, B. Podolsky, and N. Rosen. Can Quantum-Mechanical Description of Physical Reality Be Considered Complete? *PHYSICAL REVIEW Phys Rev*, 47:777, 1935.

[16] A. Ekert and R. Jozsa. Quantum computation and Shor's factoring algorithm. *Reviews of Modern Physics*, 68(3):733–753, 1996.

[17] S.J. Freedman and J.F. Clauser. Experimental test of local hidden-variable theories. *Physical Review Letters*, 28(14):938–941, 1972.

[18] A. Furusawa, J.L. Sørensen, S.L. Braunstein, C.A. Fuchs, H.J. Kimble, and E.S. Polzik. Unconditional quantum teleportation. *Science*, 282(5389):706, 1998.

[19] T. Herbst, X. Ma, W.R. Naylor, and R. Ursin, 2010. Observations made during experimental session on the Canary Islands in May 2010.

[20] C.K. Hong, Z.Y. Ou, and L. Mandel. Measurement of subpicosecond time intervals between two photons by interference. *Physical Review Letters*, 59(18):2044–2046, 1987.

[21] T. Jennewein, G. Weihs, J.W. Pan, and A. Zeilinger. Experimental nonlocality proof of quantum teleportation and entanglement swapping. *Physical review letters*, 88(1):17903, 2001.

[22] X.M. Jin, J.G. Ren, B. Yang, Z.H. Yi, F. Zhou, X.F. Xu, S.K. Wang, D. Yang, Y.F. Hu, S. Jiang, et al. Experimental free-space quantum teleportation. *Nature Photonics*, 4(6):376–381, 2010.

[23] R. Kaltenbaek. Active switching in long distance quantum state teleportation. Master's thesis, Universitaet Wien, 2003.

[24] R. Kaltenbaek, M. Aspelmeyer, T. Jennewein, C. Brukner, M. Pfennigbauer, W.R. Leeb, and A. Zeilinger. Proof-of-concept experiments for quantum physics in space. *Arxiv preprint quant-ph/0308174*, 2003.

[25] P. Kok and S.L. Braunstein. Postselected versus nonpostselected quantum teleportation using parametric down-conversion. *Physical Review A*, 61(4):42304, 2000.

[26] C. Kurtsiefer, M. Oberparleiter, and H. Weinfurter. High efficiency entangled photon pair collection in type II parametric fluorescence. *Phys Rev A*, 64:023802, 2001.

[27] P.G. Kwiat, K. Mattle, H. Weinfurter, A. Zeilinger, A.V. Sergienko, and Y. Shih. New high-intensity source of polarization-entangled photon pairs. *Physical review letters*, 75(24):4337, 1995.

[28] O. Kwon, Y.W. Cho, and Y.H. Kim. Single-mode coupling efficiencies of type-II spontaneous parametric down-conversion: Collinear, noncollinear, and beamlike phase matching. *Physical Review A*, 78(5), 2008.

[29] T.D. Ladd, F. Jelezko, R. Laflamme, Y. Nakamura, C. Monroe, and J.L. O'Brien. Quantum computers. *Nature*, 464(7285):45–53, 2010.

[30] J. Lavoie, R. Kaltenbaek, B. Zeng, S.D. Bartlett, and K.J. Resch. Optical one-way quantum computing with a simulated valence-bond solid. *Arxiv preprint arXiv:1004.3624*, 2010.

[31] P.S.K. Lee, M.P. van Exter, and JP Woerdman. Increased polarization-entangled photon flux via thinner crystals. *Physical Review A*, 70(4):43818, 2004.

[32] P.S.K. Lee, M.P. van Exter, and J.P. Woerdman. How focused pumping affects type-II spontaneous parametric down-conversion. *Physical Review A*, 72(3):33803, 2005.

[33] D. Ljunggren and M. Tengner. Optimal focusing for maximal collection of entangled narrow-band photon pairs into single-mode fibers. *Physical Review A*, 72(6):62301, 2005.

[34] I. Marcikic, H. de Riedmatten, W. Tittel, H. Zbinden, and N. Gisin. Long-distance teleportation of qubits at telecommunication wavelengths. *Nature*, 421(6922):509–513, 2003.

[35] David Mermin. Spooky actions at a distance?, 2008. Oppenheimer lecture held at the university of Berkley.

[36] M.A. Nielsen, E. Knill, and R. Laflamme. Complete quantum teleportation using nuclear magnetic resonance. *Nature*, 396(6706):52–55, 1998.

[37] J.W. Pan, D. Bouwmeester, H. Weinfurter, and A. Zeilinger. Experimental entanglement swapping: Entangling photons that never interacted. *Physical review letters*, 80(18):3891–3894, 1998.

[38] A. Peres. What is actually teleported? *IBM Journal of Research and Development*, 48(1), 2004.

[39] M. Riebe, H. Häffner, C.F. Roos, W. Hänsel, J. Benhelm, G.P.T. Lancaster, T.W. Körber, C. Becher, F. Schmidt-Kaler, D.F.V. James, et al. Deterministic quantum teleportation with atoms. *Nature*, 429(6993):734–737, 2004.

[40] M.H. Rubin, D.N. Klyshko, Y.H. Shih, and A.V. Sergienko. Theory of two-photon entanglement in type-II optical parametric down-conversion. *Physical Review A*, 50(6):5122–5133, 1994.

[41] T. Scheidl, R. Ursin, J. Kofler, S. Ramelow, X.S. Ma, T. Herbst, L. Ratschbacher, A. Fedrizzi, N. Langford, T. Jennewein, et al. Violation of local realism with freedom of choice. *Arxiv preprint arXiv:0811.3129*, 2008.

[42] E. Schrödinger. Discussion of Probability Relations Between Separated Systems. *Cambridge Phillos. Soc.*, 31, 1935.

[43] J.F. Sherson, H. Krauter, R.K. Olsson, B. Julsgaard, K. Hammerer, I. Cirac, and E.S. Polzik. Quantum teleportation between light and matter. *Nature*, 443(7111):557–560, 2006.

[44] Y.H. Shih and C.O. Alley. New type of Einstein-Podolsky-Rosen-Bohm experiment using pairs of light quanta produced by optical parametric down conversion. *Physical review letters*, 61(26):2921–2924, 1988.

[45] R. Ursin, T. Jennewein, M. Aspelmeyer, R. Kaltenbaek, M. Lindenthal, P. Walther, and A. Zeilinger. Communications: Quantum teleportation across the Danube. *Nature*, 430(7002):849, 2004.

[46] R. Ursin, F. Tiefenbacher, T. Schmitt-Manderbach, H. Weier, T. Scheidl, M. Lindenthal, B. Blauensteiner, T. Jennewein, J. Perdigues, P. Trojek, et al. Entanglement-based quantum communication over 144 km. *Nature Physics*, 3(7):481–486, 2007.

[47] L. Vaidman. Teleportation of quantum states. *Physical Review A*, 49(2):1473–1476, 1994.

[48] G. Weihs, T. Jennewein, C. Simon, H. Weinfurter, and A. Zeilinger. Violation of Bell's inequality under strict Einstein locality conditions. *Physical Review Letters*, 81(23):5039–5043, 1998.

[49] M. Żukowski, A. Zeilinger, M.A. Horne, and A.K. Ekert. "Event-ready-detectors" Bell experiment via entanglement swapping. *Physical Review Letters*, 71(26):4287–4290, 1993.

[50] W.H. Zurek and W.K. Wootters. A single quantum cannot be cloned. *Nature*, 299(802):66, 1982.

# Acknowledgments

This thesis simply would not have been possible without the help of many people. First I would like to thank everyone in the group of Anton Zeilinger and in general everyone who comes through our kitchen here at Boltzmanngasse. In particular I must thank Anton Zeilinger, who has provided much support and an inquisitive atmosphere, and Xiaosong Ma, who knows more tricks in the lab than I ever imagined would exist.

And one needs a little of something other than the precise inquisition into the reality of nature (or is it the nature of reality) to stave off insanity and thus my thanks also go out to all the people that have passed through my life in my time here in Vienna. I don't dare begin to list names for fear I won't stop and then when I do I will have forgotten the most important one.

Finally, to the olds, thanks.

# Curriculum Vitae

William Robb Naylor
1/3076/4 Molkereistraße
1020
Wien
Österreich

*Ph:* +43 676 404 6631
*Email:* willrnaylor@gmail.com

## Personal Information

Research Assistant                    *Born:* 24 June 1985, Clyde, New Zealand
IQOQI                                      *Nationality:* New Zealander
Wien                                        *Marital Status:* Single

## Education

**Universität Wien**, Vienna, Austria.

> M.Sc., Physics, 2009 - 2010.
> Expected graduation date, November, 2010.
> Also studied German language, obtaining CEFR level B2-1.

**University of Otago**, Dunedin, New Zealand.

> B.Sc. (Hons) - First Class, Physics, 2005 - 2008.
> $A^+$ average over all years (based on percentage grades averaged over all years).

**Victoria University of Wellington**, Wellington, New Zealand.

> Completed first year architecture course but chose not to pursue further studies, 2004.

## Honours and Awards

Beverly Bursary in Physics, 2006, 2007, 2008.
Prestige Scholarship in Science, 2007.
R.J.T. Bell Prize in Mathematics (shared), 2006.

## Work Experience

**University of Otago,** Dunedin, New Zealand.

*Undergraduate Demonstrator:* **March 2007 - Oct. 2008**
- Phsi 132 *Fundamentals of Modern Physics*, July 2008 - Present.
  Laboratory demonstrator and tutorial supervisor in first year course.
- Phsi 365 *Computational Physics*, March - June, 2008.
  Teaching assistant in third year computational physics tutorials.
- Phsi 131 *Physical Law and Its Applications*, March - June, 2008.
  Laboratory demonstrator in first year course.
- Phsi 191 *Biological Physics*, March - June, 2007.
  Laboratory demonstrator in first year physics course aimed at medical under-graduates.

**The Australia National University,** Canberra, A.C.T. Australia.

*Research Assistant:* **Nov 2007 - Feb 2008.**
Department of Nuclear Physics. Supervisors: Mahananda Dasgupta and David Hinde. Mostly computational work on low energy fission angular distributions.

**Victorian eResearch Strategic Initiative, VeRSI,** Melbourne, Vic. Australia.

*Computer Programmer:* **Nov 2006 - Feb 2007.**
Work in conjunction with The University of Melbourne on iTunesU. Work on the educational virtual beamline (eVBL) installed at the Australian Synchrotron.

**Miscellaneous.**

Have worked numerous part time jobs unrelated to the study of physics beginning in 1993 selling my own art. Other jobs include a gardener, fruit picker, vineyard worker, heavy construction labourer, builders labourer, painter, bar staff and newspaper delivery boy.

## Computational Skills

*Languages:* MATLAB, Objective-C, Python, XML.
*Operating Systems:* Unix/Linux, Windows.

## Publications

*Papers:*
- Patrick M. Ledingham, **William R. Naylor**, Sarah E. Beavan, Matthew J. Sellars and Jevon J. Longdell, *Non-classical photon streams using rephased amplied spontaneous emission: The role of inhomogeneous broadening in DLCZ*

*schemes*, Phys. Rev. A, vol. 81, issue 1, 2009.

- Xiaosong Ma, Borivoje Dakic, **William R. Naylor** Anton Zeilinger and Philip Walter, *Experimental analogue quantum simulation*, submitted to Nature, 2010.

*Poster Presentations:*

- **William R. Naylor** and Jevon J. Longdell, *Characterisation of a two-pulse photon echo,* presented at the Dan Wall symposium, Queenstown, New Zealand, 2008.
- Xiaosong Ma, **William R. Naylor** and Anton Zeilinger, *Long distance quantum state teleportation,* presented at the SFB meeting, Innsbruck, Austria, 2010.
- Xiaosong Ma, Borivoje Dakic, **William R. Naylor** and Philip Walter, *Quantum simulation of valence bond state,* presented at the SFB meeting, Innsbruck, Austria, 2010.

## General Interests:

Played basketball throughout high school and have coached two seasons of mini-ball and one season of representative basketball.

Played soccer from 1993 - 2008.

Have played guitar since 2000.

My main recreation currently is running. I completed the 2009 Amsterdam marathon (although was injured at the time) and am currently training for the 2010 Budapest marathon. My P.B. half marathon time is 1:27:22.

And of course as a scientist I am interested in the world around us and how it works.